Estuarine, Coastal and Shelf Science 329 (2026) 109668

Contents lists available at ScienceDirect

Estuarine, Coastal and Shelf Science

journal homepage: www.elsevier.com/locate/ecss

Bivariate extreme analysis for coastal flooding in the Adriatic Sea☆

Sara Corvaro, Francesco Marini *, Stefania Rocchi, Carlo Lorenzoni

Università Politecnica delle Marche, Department of Construction, Civil Engineering and Architecture (DICEA), Via Brecce Bianche 12, Ancona, 60131, AN, Italy

ARTICLE INFO

Keywords:
Storm surge
Wave height
Bivariate extreme statistical analysis
Coastal flooding risk
Climate change

ABSTRACT

This study investigates the interaction between storm surge and wave height in the Adriatic Sea, focusing on their combined joint influence on coastal flooding risk under different climate scenarios and return periods. Using bivariate statistical analysis based on measured data (water levels) and hindcast data (significant wave heights), the research quantifies the joint probabilities of extreme storm events and highlights the contribution of waves (wave set-up) in amplifying extreme sea levels (ESLs) in the coastal area. In particular, the study aims to assess extreme sea levels in the Adriatic Sea by providing ESLs maps for different return periods and two IPPC climate change scenarios (SSP1-1.9 and SSP5-8.5). Maximum ESLs are observed in the northern Adriatic, with Venice identified as a hotspot. Wave contributions are shown to substantially double water levels, particularly in the areas between Ancona and Zadar and near the southern entrance at Otranto, emphasizing the need for a bivariate approach to accurately capture these interactions. The projected sea level rise further exacerbates the risks posed by storm events, particularly for vulnerable coastal areas. The present study underscores the need for a more comprehensive understanding of the combined joint effects of storm surge and waves, and enable more effective coastal flooding risk assessments along the Adriatic coast due to extreme sea levels by providing valuable support for designing mitigation measures to address climate-driven extreme events.

1. Introduction

Many coastal phenomena, such as overtopping, loads on structures, and coastal flooding, arise from the combined action of multiple physical drivers, including sea level, waves, currents, and winds. The Adriatic Sea, a semi-enclosed Mediterranean sub-basin, is an ideal environment to investigate these interactions due to its elongated geometry, limited tidal range, and sensitivity to meteorological forcing. Consequently, the basin is particularly prone to significant environmental changes during extreme events.

Several studied have analyzed extreme sea-levels in the Adriatic Sea. Šepić et al. (2022) decomposed positive and negative sea level extremes into seven components forced by different processes. They found significant differences between the northern and middle/southern Adriatic extremes and between positive and negative extremes. The study of Ruić et al. (2023) showed that high-frequency sea level oscillations (2 min< T <2 h) can considerably contribute to positive sea level extremes. Another fundamental aspect of the Adriatic Sea's dynamics is tidal resonance, a phenomenon where the natural oscillation period of the basin coincides with tidal forcing, leading to amplified tidal effects. The work of Medvedev et al. (2020) provides observational evidence of tidal resonance in the Adriatic Sea due to its elongated shape and shallow depths, emphasizing its significant impact on local sea level variability. Cushman-Roisin and Beckers (2011) and Malačič et al. (2000) studied the tidal dynamics in the Adriatic Sea and they identified the key resonance frequencies that amplify the tidal range in specific areas of the basin. The sensitivity of the Adriatic Sea to resonance phenomena plays a crucial role in storm surge amplification, particularly during extreme weather events when the combination of meteorological forcing and resonant conditions can significantly elevate the sea levels. Cushman-Roisin et al. (2013) demonstrated how storm-induced sea level rises are exacerbated by resonant conditions, particularly in the northern part of the Adriatic Sea, due to the geometry and the shallow water depth of the area. Understanding these interactions is essential for coastal management, especially in the context of climate change, which is expected to increase the frequency and intensity of extreme events in the Adriatic region. Studies such as Lionello et al. (2006) highlight the importance of incorporating both meteorological and tidal processes in forecasting models to better predict extreme sea level events. As the scientific community continues to refine its models, the insights provided by Medvedev2020 and related research offer critical guidance for improving the resilience of coastal communities along the Adriatic coast. Pasquali et al. (2015)

☆ This article is part of a Special issue entitled: 'The Adriatic blue growth' published in Estuarine, Coastal and Shelf Science.

* Corresponding author.
E-mail address: f.marini@staff.univpm.it (F. Marini).

https://doi.org/10.1016/j.ecss.2025.109668
Received 31 January 2025; Received in revised form 2 December 2025; Accepted 15 December 2025
Available online 16 December 2025

developed a simplified real-time method for forecasting storm surges in semi-enclosed basins like the Adriatic Sea, offering a practical approach for improving short-term forecasts during extreme events. Their study emphasized the vulnerability of the northern Adriatic to storm surges, highlighting the role of atmospheric pressure patterns and wind stress as dominant forcing mechanisms. Vousdoukas et al. (2016) evaluated storm surge levels along the European coastline for different climate scenarios. The results showed that the climate change projections lead to weakly increasing extreme values of storm surge for certain Shared Socioeconomic Pathways (SSPs) along parts of the North Adriatic Sea. Based on the extreme sea level scenarios of Vousdoukas et al. (2017) and other physical, environmental and socio-economic indicators, Furlan et al. (2021) assess the vulnerability of the Italian coast to inundation. Results show that most vulnerable areas are located in the North Adriatic, the Gargano area and other Southern parts of Italy, mostly due to the very high vulnerability scores reported by climate-related indicators (e.g. extreme sea level). Međugorac et al. (2020) studied the impact of climate change on the wind fields responsible for the Adriatic storm surges. Their analysis was based on measured sea levels in Venice and Bakar, near-surface wind from ERA5 reanalysis and simulations of wind fields. They found that the probability that the frequency, intensity, annual cycle, and spatial structure of the wind inducing the Adriatic storm surges will change in future climates is small. The impact of climate change on the storm surges of the Mediterranean Sea was also assessed by Makris et al. (2023).

In recent years, the focus has expanded from forecasting storm surges to understanding the complex interactions between different sea level components. Bivariate statistical approaches have been increasingly applied to understand such interactions in marine environments, offering enhanced insight into joint occurrences of extreme events. The adoption of multivariate statistical methods allows to take into account the occurrence probability of different extreme sea level components, such as storm surges, tides and waves. The work of Ragno et al. (2023) analyses extreme sea level events in both the Adriatic and Tyrrhenian Seas through a multivariate analyses to study the complex relationships between climatic drivers and sea level components. They found that the co-occurrence of extreme meteorological and tidal conditions can significantly increase sea level extremes, further emphasizing the need for comprehensive approaches that consider these inter-dependencies when assessing coastal risks. Multivariate methods, as highlighted by Ragno et al. (2023), are crucial to study how different environmental processes interact to produce extreme events. Other multivariate analyses consider the sea levels, driven by storm surges, and the wave heights, occurring simultaneously with these elevated levels, as the main variables. In many cases, failure to address both aspects can lead to underestimations of the risks associated with extreme coastal events. These approaches can improve the accuracy of hazard models and support more effective coastal management strategies, particularly in regions like the Adriatic Sea, where the combined effects of storm surges, tides and wave action are particularly significant. Joint statistical analyses of storm surge and wave conditions have been applied not only in Europe (e.g.; Petroliagkis, 2018; Galiatsatou and Prinos, 2016), but also extensively around the world, including tropical and cyclone-prone regions such as the South China Sea, the western Pacific and the U.S. coastline (e.g.; Haixia et al., 2023; Rueda et al., 2016; Zheng et al., 2013; Wahl and Chambers, 2015). These studies demonstrate the global relevance of multivariate frameworks for characterizing coastal extremes. However, despite the value of broad methodological advances, the dependence between surge and wave processes is strongly modulated by local morphology, meteorology and hydrodynamics, and therefore requires region-specific analyses (e.g.; Arns et al., 2017; Idier et al., 2019). Once the statistical relationship between waves and water levels has been established, the beach response to extreme events must be assessed. Several methods and parameters can be employed for this purpose (e.g. Burvingt et al., 2017; Coco et al., 2014). Some approaches are particularly suitable for broad-scale applications, as they enable a simplified evaluation of beach recession for both free beaches (e.g. Dean, 1991) and protected beaches (e.g. Marini et al., 2022).

The present study applies a multivariate copula-based analysis of storm surges and wave heights in the Adriatic Sea to provide a more comprehensive understanding of their combined impact on coastal flooding risks, accounting for the expected increase of extreme events due to climate change. As a result, the study enables an effective assessment of extreme water levels in the Adriatic Sea under different forcing conditions and provides maps of extreme sea levels for various return periods and climate-change scenarios, offering useful support for decision-makers and for the design of adaptation measures (e.g. van Gent, 2019, Marini et al., 2020).

2. Method and data analysis

2.1. Sea level components

The sea level η is composed of several components each playing a crucial role in the coastal dynamics. Orlić and Pasarić (2024) identified eight phenomena contributing to the sea level maximum. However, a comprehensive assessment of all these contributions is only feasible at a local scale, where high-resolution and site-specific data are available. Since the present study is focused on a flooding analysis extended to the entire Adriatic basin, the decomposition of each component is not of significant importance and all meteorological forcings have been included in the storm surge term. Therefore, the sea level is expressed as the sum of the contributions reported in Eq. (1). The mean sea level (η_{msl}) represents the long-term average of the sea surface height (multi-year time scale) and it can rise due to climate change (η_{slr}). Superimposed on the mean sea level are the astronomical tides (η_t), driven by the gravitational forces of the moon and sun (daily to fortnightly scale). In addition, meteorological tide or storm surge (η_{ss}) is mainly caused by changes in atmospheric pressure and strong winds during storm events and can significantly increase sea level (event scale, hours to days). The sea level adjusts to air pressure variations as an inverted barometer, such an effect is significantly larger than theoretical one in the Adriatic Sea, due to the synchronized acting of the wind and other contributors to the sea surface variability (Pasarić et al., 2000). The action of wind on the sea surface is more complex because it depends on wind speed, direction, duration and topography of the basin Vilibić et al. (2005). Finally, waves, especially during extreme weather events, raise sea levels in the surf zone through wave set-up (η_w), thereby amplifying the risk of coastal flooding (short-term variability, minutes to days).

$$\eta = \eta_{msl} + \eta_{slr} + \eta_t + \eta_{ss} + \eta_w \tag{1}$$

2.1.1. Sea level rise

According to the latest IPCC reports (Calvin et al., 2023), the likely global mean sea level rise (η_{slr}) by 2100 is between 0.28 to 0.55 m under the very low GreenHouse Gas (GHG) emissions scenario (SSP1-1.9) and 0.63 to 1.01 m under the very high GHG emissions scenario (SSP5-8).

2.1.2. Tidal levels

Tidal levels are given by two different contributions. The astronomical tide (η_t) is only due to the relative position between earth, moon and sun. It is a deterministic quantity that can be computed for each site location once the harmonic components and phases are known. The Adriatic tides can be well approximated by four semidiurnal (M2, S2, N2 and K2) and three diurnal (K1, O1, P1) harmonic constituents (Pervan and Sepić, 2023; Međugorac et al., 2018). Spreading of tides in the Adriatic is usually described by the largest M2 and K1 constituents. Semidiurnal tides have an amphidromic point halfway between Šibenik and Ancona (Pervan and Sepić, 2023). Diurnal tides are largest at

Trieste and gradually decrease moving to the southern part of the basin towards Otranto, at the entrance to the Adriatic Sea (Schwab and Rao, 1983). In addition, a strong resonance is observed in the higher diurnal tidal frequencies, especially in the northern part of the sea, close to the basin head (Medvedev et al., 2020).

The second contribution to tidal levels is driven by meteorological forcing, including the effects of wind setup, atmospheric pressure changes, and other subtidal oscillations (Orlić and Pasarić, 2024). Collectively, these contributions are referred to as "storm surge" (η_{ss}). The storm surge component is usually computed as the difference between the observed sea level (SL) and the astronomical tide. However, this definition cannot adequately represent the meteorological contribution in case of large residuals due to the non-linear interaction between tide and surge which induces a phase shift in the tidal signal (Williams et al., 2016). Recent studies highlight that nonlinear tide–surge interactions can be explored using different methodological frameworks. Statistical Tide–Surge Interaction (TSI) methods quantify how the non-tidal residual varies with tidal level or phase (e.g.; Bernier and Thompson, 2007; Jenkins et al., 2025), and are particularly effective in macrotidal environments where such modulation is pronounced, though they may still offer complementary insights in microtidal settings. In parallel, non-stationary tidal analysis tools, such as NS_TIDE (Matte et al., 2013), explicitly incorporate time-varying tidal constituents and have been developed to account for tide–river interactions, with recent applications also in Adriatic river–sea systems (e.g.; Krvavica et al., 2025). While these approaches provide detailed diagnostics of non-linearity, their implementation typically requires long records, high-frequency measurements, or dedicated calibration. In the present study, a simpler but robust and widely adopted indicator is therefore preferred, namely the "skew surge" (de Vries et al., 1995), to identify the meteorological contribution, although it does not capture all forms of nonlinearity (e.g., phase-dependent residuals or low-frequency modulation of tidal constituents). Skew surge is computed as the difference between the maximum observed SL and the predicted high astronomical tide within a tidal cycle, independently of the time occurrence. The skew surge is used as a practical indicator of the meteorological contribution to sea-level extremes (e.g.; Williams et al., 2016; Stephens et al., 2020) and it has also been applied in studies of the Adriatic Sea (e.g.; de Vries et al., 1995; Paprotny et al., 2016, 2020; Ragno et al., 2023; Baldoni et al., 2025). According to its definition, a single value of skew surge within a tidal cycle is computed; which is, by definition, lower than the maximum tidal residual. However, the authors highlight that this approach can lead to a strong underestimation of the skew surge values when the peak of the storm surge occurs in correspondence to the lower tide levels. To overcome this limitations, a hybrid approach is used in the present study, where the storm surge is computed as skew surge for the tidal phases around relative tidal maximal levels and as tidal residual around minimal levels. This method avoids the underestimation of storm surge levels when sea-level rise occurs during low-tide conditions. An example of the application of this hybrid approach is shown in Fig. 1. Two different events are considered: one in which the maximum measured water level coincides with low tide (Panels a and c), and another in which it coincides with high tide (Panels b and d). Panels a and b display, for each case, the measured water levels (blue line) and the astronomical tide (red line). Panels c and d show the tide residuals (black) and the skew surge in both its classical (cyan) and hybrid (magenta) forms. This figure highlights the advantages of adopting the hybrid approach. The classical skew surge performs well when the water level peak occurs near high tide, as indicated by the close agreement among the three curves in Panel d. Conversely, when the storm surge peak occurs during a low-tide phase (Panel a), the difference between the residual and the skew surge becomes large, and the classical skew surge tends to underestimate the actual surge level. The hybrid approach combines the strengths of both definitions: it accounts for nonlinear effects near high tide while avoiding underestimations when surges develop during low-tide conditions.

2.1.3. Wave setup

The last contribution reported in Eq. (1) is due to wave effects. Short wave periods are in the order of 10 s, approximately 4000 times smaller with respect to those of tides ($\approx$ 12 h). For design purposes, a typical sea-state is usually assumed to last for 3 h (Det Norske Veritas, 2021) and it is represented by the significant wave height (H_s). The influence of waves on the variation of the mean sea level has to be taken into account within the surf-zone. Wave set-up is the time-averaged increase in the mean sea level due to breaking waves. The wave setup can be evaluated by means of Bowen's (Bowen et al., 1968) formula, which is valid for all beach profiles. The wave setup is about 19% of the breaking wave height H_b (as reported in Dean and Dalrymple 1991) at the still-water shoreline. The maximum value of the wave setup depends on the local emerged beach profile and it is site-specific dependent. The value of the wave height at the breaking depth is influenced by both the meteo-marine and geometric conditions. Indeed, the wave transformation processes from deep waters to shore are influenced by different parameters such as wave period, wave direction, bathymetry, water depth at the breaking point h_b. The breaking wave height is given by the product of the shoaling coefficient k_s, the refraction coefficient k_r and the offshore significant wave height H_s. For random waves, the shoaling coefficient from deep waters to breaking conditions is about in the range 0.93–1.5, while the refraction coefficient is about in the range 0.7–1.0 (Goda, 2010).

2.2. Data collection

2.2.1. Mean sea level and sea level rise

The mean sea level may refer to different local reference systems (e.g. Italian and Croatian), hence, to facilitate comparisons across different locations, η_{msl} is removed from the current analysis. However, to obtain a local estimate of the total sea level, the mean sea level value must be added back at each site at the end of the analysis.

To assess sea level rise effects on total levels, the NASA Sea Level Projection tool (https://sealevel.nasa.gov/ipcc-ar6-sea-level-projection-tool) is used to show the median projections along the Adriatic Sea depending on the IPCC gas emission scenario. It is found that the expected sea level rise varies in the range 0.29–0.42 m for SSP1-1.9 and 0.64–0.78 m for SSP5-8, in substantial agreement with global projections.

2.2.2. Astronomical tide and storm surge

The present study makes use of real data from 12 different stations of the national tide gauge networks of Italy and Croatia to isolate the contributions of astronomical tide and storm surge (meteorological tide) from sea-level measurements, as shown in Fig. 2. The Italian tide gauge network is managed by the National Institute for the Environment Protection and Research (ISPRA) (https://www.mareografico.it/), while the Croatian tide gauge network is managed by the Hydrographic Institute of the Republic of Croatia (HHI) (https://adriaticsea.hhi.hr/). All tide gauges are located in positions where the wave movement can be assumed negligible (port, lagoon, etc.). The dataset consists of long-term sea-level records with a temporal resolution of either 1 h or 10 min, spanning different durations. Table 1 shows the length of sea level recordings measured by the selected tide gauges. Some recorded years are not considered in the analysis because the data quality was poor, due to a large number of missing data (fragmented time series). In Table 1 the main dataset characteristics used for the present bi-variate statistical analysis are also reported as the number of years N_y, the number of joint storm events N (the selection of joint events will be explained in Section 2.3.3) and their ratio $\lambda = N/N_y$.

A more comprehensive assessment of the Adriatic Sea would require sea-level data from the Montenegrin and Albanian coasts to better evaluate the behavior of its southern part. However, such data were unavailable for a sufficient duration or resolution to allow for extreme value analysis.

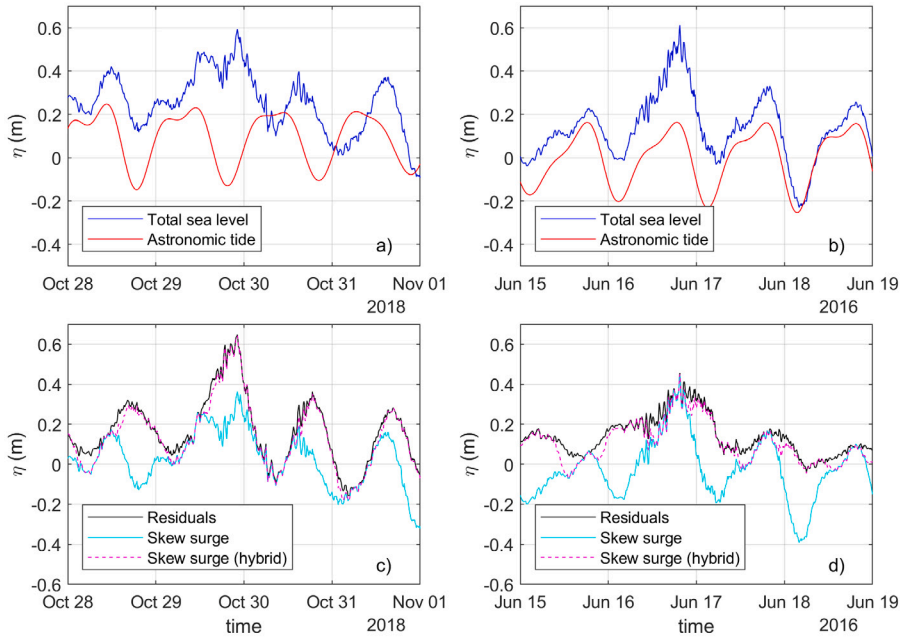

Fig. 1. Application of the hybrid approach for storm surge identification to two different surge events, in phase with low tide (Panels a and c) or high tide (Panels b and d), respectively. Panels a and b show the total level and the astronomic tide, while Panels c and d show the residuals, the skew surge and the hybrid skew surge. (For interpretation of the references to color in this figure legend, the reader is referred to the web version of this article.)

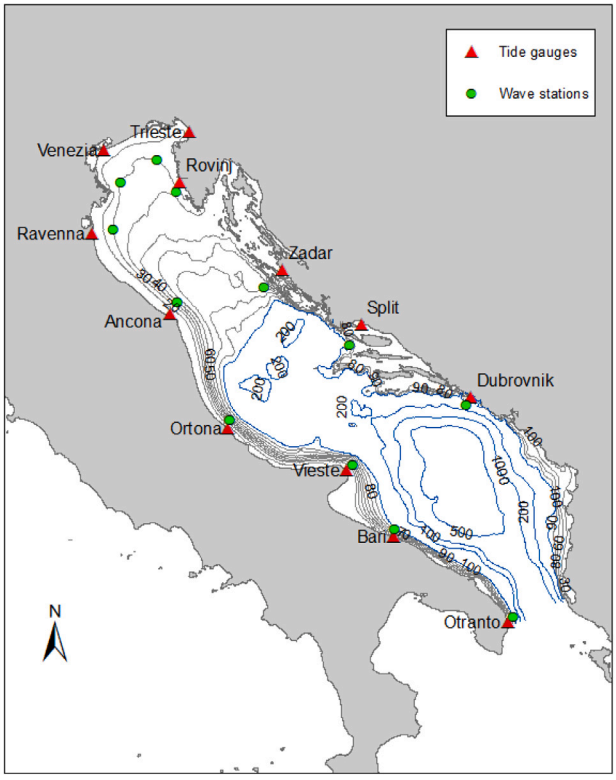

Fig. 2. Tide gauges locations (red triangles) of the Italian and Croatian tide gauge networks and wave stations (green circles) of the CMEMS model. (For interpretation of the references to color in this figure legend, the reader is referred to the web version of this article.)

Table 1
Length of the time series, number of years N_y, number of joint storm events N and $\lambda = N/N_y$.

Stations	Length of time series	N_y	N	λ
Venezia	1998; 2002–2022	22	184	8.4
Trieste	1994; 1997–1998; 2002–2016; 2019–2022	22	271	12.3
Ravenna	2002–2014; 2020–2022	16	200	12.5
Ancona	1997–1998; 2002–2023	24	255	10.6
Ortona	2003–2009; 2011–2016; 2020–2022	16	145	9.1
Vieste	2003–2017; 2020–2022	18	210	11.7
Bari	2003–2014; 2020–2022	15	162	10.8
Otranto	2003–2022	20	248	12.4
Rovinj	1956–2013; 2015–2016	24	366	15.3
Zadar	1996–2015; 2017–2019	23	355	15.4
Split	1956–1992; 1994–2016; 2018–2019	25	469	18.8
Dubrovnik	1957–1959; 1961–1990; 1993–2010; 2012–2017	24	368	15.3

2.2.3. Wave height

The Italian national wave buoy network (ISPRA) has only 3 wave buoys in the Adriatic Sea (Venice, Ancona and Ortona), while wave data are not available from the Croatian national network, hence the spatial consistency from measured data is very poor. Moreover, wave data records (from wave buoys) do not cover long overlapped periods with sea-level records (from tide gauges), indeed in-situ wave observations are few and often temporally fragmented. In order to maximize the dataset length reported in Table 1, computed wave data from the wave reanalysis dataset of the Copernicus Marine Service (CMEMS: https://data.marine.copernicus.eu/product/MEDSEA_MULTIYEAR_WAV_006_012) were used in the present study. This dataset is a multi-year wave reanalysis starting from January 1993, composed by hourly wave parameters at 1/24° horizontal resolution, covering the Mediterranean Sea and it includes an optimal interpolation scheme assimilating significant wave height along track satellite observations of CMEMS. The time series of CMEMS overlap very well with the tide gauge recordings, mainly for the Italian side. Unfortunately, the sea level recordings of three Croatian stations (Rovinj, Split and Dubrovnik) prior to 1993 are not taken into consideration in the present study due to the lack of overlapped periods with wave height data.

The CMEMS model reproduces well the significant measured wave height (SWH), with typical Root-Mean-Squared-Difference (RMSD) values of about 0.23–0.24 m and BIAS values around –0.05 m, corresponding to a relative error of 4%–7% with respect to observations.

Table 2
Characteristic values of significant wave height (H_s) and peak period (T_p) at selected Adriatic sites. Reported parameters include the mean, the 75th and 90th percentiles (q75, q90) and the maximum value from each time series.

Site Name	H_s (m)				T_p (s)			
	mean	q75	q90	max	mean	q75	q90	max
Venezia	0.51	0.66	1.13	5.29	3.98	4.74	6.30	16.35
Trieste	0.40	0.52	0.90	4.52	3.48	4.31	5.73	14.86
Ravenna	0.54	0.69	1.18	4.94	4.12	5.21	6.30	14.86
Ancona	0.57	0.74	1.20	5.03	4.22	5.21	6.93	12.28
Ortona	0.54	0.69	1.12	5.25	4.46	5.21	6.30	12.28
Vieste	0.75	1.00	1.50	5.39	4.47	5.21	6.30	12.28
Bari	0.61	0.80	1.25	4.78	3.47	5.21	6.30	12.28
Otranto	0.79	1.04	1.62	6.23	5.15	6.30	7.63	13.51
Rovinj	0.40	0.52	0.83	4.60	3.96	4.31	6.30	16.35
Zadar	0.53	0.66	1.11	5.53	3.96	4.74	7.34	14.86
Split	0.42	0.53	0.90	4.10	3.98	4.74	6.30	14.86
Dubrovnik	0.53	0.66	1.15	5.48	4.77	5.73	7.63	14.86

The model tends to slightly underestimate SWH, especially for low and intermediate waves, while higher waves are generally well reproduced. For the Adriatic Sea, the validation performed for the reanalysis period (1993–2018) shows mean BIAS values of -0.108 ± 0.032 m and -0.135 ± 0.027 m, and RMSD values of 0.281 ± 0.018 m and 0.277 ± 0.021 m, for the northern (adr1) and southern (adr2) subregions, respectively. The model validation is extensively documented in the CMEMS quality information document (https://documentation.marine.copernicus.eu/QUID/CMEMS-MED-QUID-006-012.pdf).

To accurately represent the climate conditions at each site, the wave stations are selected in different points with respect to the tide gauges, in order to be associated with open sea wave conditions. Each wave station is chosen at a water depth (larger than 30 m) deep enough to be far from shallow water wave conditions and, at the same time, at a limited distance (from 10 km to 50 km) from the shoreline (and the corresponding tide gauge location) to be able to relate open sea wave motion with tideographic effect (joint events). In addition, to ensure that the selected locations are not significantly affected by coastal proximity or by the presence of nearby islands, a set of characteristic wave parameters was computed for each site. Significant wave height (H_s) and peak period (T_p) were considered as representative variables. From the time series of each variable, four characteristic values were derived: the mean, the maximum and two percentile-based values corresponding to the 75th (q75) and 90th (q90) percentiles. These parameters provide a concise description of both the average and the extreme wave conditions at each site. The resulting values are summarized in Table 2. Although some of the selected points are located near sheltered coastal areas or close to complex island environments, their characteristic wave parameters (Table 2) are consistent with those derived at nearby and more exposed sites. In particular, the mean and percentile values (q75 and q90) of significant wave height (H_s) and peak period (T_p) fall within the same range observed for offshore stations along the Adriatic coast. Therefore, the selected points can be considered representative of the regional wave climate.

2.3. Extreme value statistical analysis

The statistical analysis aims to study the existing relations between different sea level components. Among them, the sea level rise due to climate change is associated to the time scale of years so it can be treated as a stand-alone component according to the results of the latest IPCC report (Calvin et al., 2023). Since the astronomical tide is a deterministic quantity, the multivariate statistical analysis has been applied to two variables: the storm surge and the significant wave height. To identify the contribution of storm surge and waves to Extreme Sea Levels (ESL), the following procedure was applied to each site:

1. reconstruct the astronomical tide components from the measured sea levels by the tide gauges and compute the storm surge as the residual;
2. choose the best threshold (specific for each site) for data declustering to identify an adequate number of independent events;
3. apply the Peak Over Threshold (POT) analysis to storm surge dataset;
4. find the wave height values associated with each storm surge event and evaluate the extreme distributions of wave height dataset;
5. model the joint distribution of storm surge and wave height following a copula-based approach;
6. show the results in the form of environmental contours.

In the following Sections, each step is described in detail.

2.3.1. Astronomical tide and storm surge's computation

The tidal components, such as spring tides and neap tides, were identified by using the MATLAB-based tool "Tidalfit" (Grinsted, 2014). This tool enables an analysis of tidal harmonics, breaking down the signal measured by the tide gauge into its constituent parts. The determination of the amplitude and phase of each component allows the computation of the astronomical tide time series at each location. In particular, "Tidalfit" applies the HAMELS (ordinary least squares) method to fit the tidal signal. The tool automatically selects all harmonic constituents whose periods are shorter than one quarter of the data time span and longer than twice the sampling interval, resulting in a total of 38 astronomic tidal components used for the reconstruction of the tidal time series. From the computed astronomical tidal level, the Mean Higher High Water (MHHW), which is the average height of the higher daily high tides, was evaluated and it can be considered a representative value of the high tides recorded at each site. MHHW reflects high tide levels that occur more frequently and avoids overestimating combined effects when considering multiple environmental variables. For this reason, it is usually worldwide employed in mapping inundation due to extreme events (Schmid et al., 2014; Phillips, 2024) or to sea level rise (Sweet et al., 2018). The effect of climate change on astronomical tide sea levels is disregarded because, except in specific cases, regional changes in tides are negligible in comparison to the other ESL components, according to Vousdoukas et al. (2018).

After computing the astronomical tidal levels, the storm surge time series is computed according to its definition given in Section 2.1.2.

2.3.2. Threshold identification and POT analysis for storm surge data

An appropriate threshold has been selected for each site in order to identify the storm surge peaks of the extreme value analysis. Although several studies recommend automatic threshold selection algorithms (Bader et al., 2017; Callahan and Leathers, 2021), in this study a range of thresholds was studied, starting from the 90th percentile of storm surge and above, where extreme values tend to dominate. Several approaches can be used to ensure that storm surge events are independent. Martín et al. (2024) studied the temporal evolution of extreme events measured at 1485 tide gauge records from across the global coast, highlighting a notable variability of the Standard Event Duration (SED) ranging from 20 h to 140 h. Ragno et al. (2023) applied a constant declustering time equal to 48 h for both the Adriatic and Tyrrhenian Seas. Zachary et al. (1998) showed that taking a period length larger than 48 h is not necessary to ensure that the associated observations can be treated as independent. In the Adriatic Sea, storm surges mostly occur when a low atmospheric pressure is conjoined with strong south-eastern winds (Scirocco) blowing and pushing water mass for hours or days towards the northern part of the Adriatic Sea, as reported in Pervan and Sepić (2023). The duration of the largest extreme storm events observed in their study ranges from about 2 h to 45 h. Storm surge events must be separated by at least 24 h, in order to exclude the occurrence of repeated extreme sea levels due to

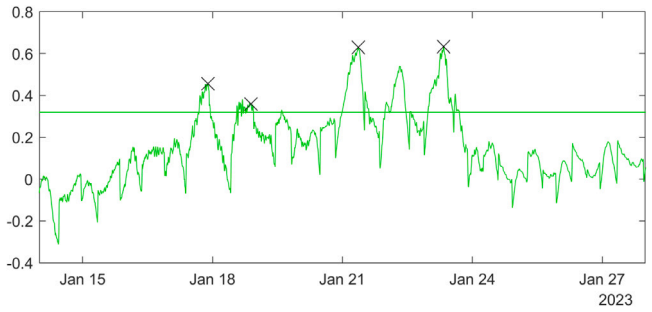

Fig. 3. Storm surge peaks (black crosses) individuated after the declustering phase.

moderate storm surges reinforced by the Adriatic-wide seiche, with a principal period of about 21.5 h. Therefore, the present study considers two different durations for the declustering procedure: 24 h and 48 h. The extreme storm surges and wave heights for the duration of 24 h and 48 h associated with a Return Period of 100 years are compared, considering the 48 h case as representative of independent events. Choosing the duration of 24 h for data declustering, the maximum absolute error in extreme waves and surge is 11.1%, with a mean absolute error of 2.9% and a standard deviation of 3.2%. Due to the small differences between the two declustering methods, a storm surge duration of 24 h was chosen to increase the number of storm events by 31.2%. This ensures a sufficiently long dataset for multivariate analysis and allows an accurate evaluation of the dependence between variables, as suggested by Mazas and Hamm (2017). An example of the declustering procedure to separate individual storm surge peaks from the broader dataset is reported in Fig. 3.

For each declustered set of storm surge peaks associated with a specific threshold, the *Generalized Pareto* (GP) distribution is used and the following criteria were applied to choose the best threshold:

- the *Mean Residual Life* (MRL) plot in which the mean observed excess over the threshold is plotted against the threshold itself. If the *Generalized Pareto* (GP) assumption is correct, this plot shows a linear trend (Davison and Smith, 2018);
- the trends of the shape (k) and scale (σ) (GP) parameters. A well-established practice (Scarrott and MacDonald, 2012) considers that the parameters tend to exhibit linearity up to a certain point, deviations from this behavior can indicate where the threshold should be set;
- the evolution of the *Normalized Root Mean Square Error* (NRMSE). A scatter in the NRMSE plot indicates that a lower threshold should be set.

The MRL is computed as the expected value, $E(\cdot)$, of the observed values y_o larger than a specific threshold y_t, according to Guess and Proschan (1988):

$$MRL(y_t) = E[y_o - y_t | y_o > y_t] \tag{2}$$

The GP parameters (k and σ) are obtained by the Maximum Likelihood Estimation (MLE) and the NRMSE is computed according to the following equations:

$$NRMSE = \frac{RMSE}{\bar{y}} \tag{3}$$

$$RMSE = \sqrt{\frac{\sum_{i=1}^{N}(y_o - y_d)^2}{N}} \tag{4}$$

where y_d are the distribution values, N is the number of samples in each cluster and $\bar{y}$ is the mean of y_o.

The fitting of the Generalized Pareto (GP) distribution to the storm surge data cluster with a chosen threshold allows to predict extreme events associated with different Return Periods (RPs). The k and σ parameters of the optimal GP distribution are estimated with the MLE by using the *gpfit* MATLAB function (The MathWorks Inc., 2024).

2.3.3. Extreme statistical distributions for wave height dataset

To accurately model the relationship between wave heights and storm surge peaks, the first step was to associate wave height values to the storm surge cluster. Once the peak time of the storm surge is identified, the corresponding wave height is determined. As reported in Mazas and Hamm (2017), it is recommended to select the maximum wave height value within a time window centered on the storm surge peaks. In this study, a time window of ±5 h is used. Such a time window is needed because the sea states are available offshore, while the sea levels are measured onshore (e.g. at a tide gauge), hence the wave propagation time should be accounted for. Moreover, as reported above, non-linear interaction between different sea level components induces a phase shift in the sea level signals.

This procedure allows to obtain a set of storm surge-wave height pairs. In coastal engineering, it is common practice to exclude pairs of values associated with less intense energetic conditions, hence it consists of using multivariate thresholds. As reported in Mazas and Hamm (2017), and in Li et al. (2014) an event (i.e. a storm) is defined when both storm surge and wave height exceed their threshold values. The choice of statistical thresholds is based upon statistical criteria, such as those described by Bernardara et al. (2011), close to 95th percentile of the data. Since a correct application of the extreme statistical distribution of wave heights requires a dataset composed of extreme data, a limit level for wave heights is also needed. Observations of the wave regime in the Adriatic Sea show that waves resulting from breeze regimes do not reach values of significant wave height larger than 1 m, while waves generated by atmospheric disturbances exceed such limit. These observations are also confirmed by the 90th percentile values of the significant wave height (H_s) evaluated at wave stations along the Adriatic Sea reported in Table 2. Therefore, a threshold of 1 m for the wave height data is applied in the present study.

Once threshold values are chosen, the final cluster of N samples (joint events) is identified over the effective number of years of observations N_y (as reported in Table 1) and the mean number of selected events per year (λ) is defined as:

$$\lambda = N / N_y \tag{5}$$

Following Mazas and Hamm (2017), optimal values of N and λ depend on the type of application. For the univariate case, depending on the duration of time series, which is usually 20–25 years in engineering applications, values of λ between 5 and 10 are needed to have a sample size larger than 100 (Mazas and Hamm, 2011). For the multivariate case, more information is necessary to correctly evaluate the dependence between variables. The sample size should then be increased up to values of λ in the range 15–25, depending also on the duration of the time series and on the physical processes under study. The number of years of observation is larger than 15 years for all the locations. The values of λ, reported in Table 1, are slightly lower than the suggested values but, for each case, the total number of joint events is in the range 150–500, thus allowing an accurate evaluation of the joint probability of occurrence of extreme events.

Once each cluster of data is identified the Generalized Pareto distribution is applied to the updated storm surge dataset, while, for the wave height dataset, the best extreme statistical distribution is sought among several candidates (Gumbel, Weibull, Log-Normal, Generalized Extreme Value (GEV), Gamma distributions). Each of these distributions has distinct characteristics that make them suitable for modeling extreme environmental variables. For instance, the Weibull distribution is commonly used in wave height studies due to its flexibility in representing various types of data, while the GEV distribution is a natural choice for extreme value analysis. To determine the best fit,

the RMSE was computed according to Eq. (4) between the observed wave height values and those predicted by each distribution. The RMSE provides a measure of the differences between predicted and actual data points, with lower values indicating a closer match between the distribution and the observed data. Using RMSE as the criterion for optimal fit ensures that the selected distribution accurately represents the variability in the observed wave height data.

2.3.4. Copula distribution

After determining the marginal distribution for the second variable (in this case, wave heights), the next step is to model the dependence structure between the two variables, storm surge and wave heights. Such joint distribution was modeled using a copula approach, which allows to model the dependency between random variables separately from their marginal behaviors (Nelsen, 2006). Given the marginal distributions F_x and F_y of two random variables X and Y, the copula $C(\cdot,\cdot)$ is an operator that relates the two marginal distribution with their joint distribution F_{xy}, according to the Sklar's theorem (Sklar, 1959):

$$F_{xy}(X,Y) = C(F_x(X), F_y(Y)) \tag{6}$$

In other words, each pair of real numbers (X,Y) leads to a point $(F_x(X), F_y(Y))$ in the unit square $[0,1]\times[0,1]$ and this pair corresponds to a number $F_{xy}(X,Y)$ in the interval $[0,1]$.

In this study, the variable X corresponds to the storm surge and its marginal distribution F_x is modeled as a Generalized Pareto (see Section 2.3.2), while the variable Y corresponds to the wave height with marginal distribution F_y coming from Section 2.3.3. Several copula types were tested, including Archimedean copulas, such as Gumbel, Clayton, and Frank, which are often used for their simplicity and ability to capture various dependency structures, especially in the tails of distributions. Additionally, elliptical copulas were explored, specifically the Student's t copula, generally used to model symmetric dependence and heavier tails, which are common in environmental data. The parameters of these copulas were estimated using the MATVines tool (Coblenz, 2021), which is specifically designed for vine copula modeling. This tool provides a systematic way to fit and evaluate the copulas based on the available data. To select the best copula type, the Akaike Information Criterion (AIC) was applied, which is a widely used method for model selection that balances goodness of fit with model complexity. It is defined as:

$$AIC = 2(k - \ln(L)) \tag{7}$$

where L is the likelihood function and k is the number of parameters in the copula model used to favor models with less number of parameters. The copula that minimized the AIC was chosen as the best representation of the dependency between storm surge and wave heights, allowing for a more accurate and flexible joint modeling of these variables.

2.3.5. Environmental contours

The copula-based analysis requires a tool to describe and graphically represent the joint behavior of the analyzed parameters. The most popular is based on the inverse Rosenblatt transformation and consists in the Inverse First-Order Reliability Method (IFORM) (Winterstein et al., 1993). These contours are essential tools in offshore and coastal engineering, providing insights into the joint occurrence of extreme environmental conditions at specific RPs (Eckert-Gallup et al., 2016; Saranyasoontorn and Manuel, 2004; Huang and Dong, 2021; Baldoni et al., 2025). For a given return period RP, the associated reliability index (β) is computed as a function of the exceedance probability (p_f) as:

$$\beta = -\phi^{-1}(p_f) \tag{8}$$

where ϕ is the cumulative distribution function of a standard normal variable. The exceedance probability, for RP relatively large, can be computed as:

$$p_f = \frac{1}{\lambda RP} \tag{9}$$

where λ is the mean number of events per year. An environmental contour is given by the pairs Z_x and Z_y defined along the circle:

$$\sqrt{Z_x^2 + Z_y^2} = \beta \tag{10}$$

Z_x and Z_y are random variables obtained from the Rosenblatt transformation (Rosenblatt, 1952). From Z_x and Z_y, the random variables U_x and U_y uniformly distributed on $[0,1]$ can be computed as:

$$U_x = \phi(Z_x) \tag{11}$$

$$U_y = C^{-1}(\phi(Z_y)|\phi(Z_x)) \tag{12}$$

where $C^{-1}_{y|x}$ is the inverse conditional distribution function (inverse h-function of Aas et al. 2009) of the copula and it can be computed numerically (Coblenz, 2021) or from specific expressions for frequently used copula models (Montes-Iturrizaga and Heredia-Zavoni, 2015). Once the pairs U_x and U_y are computed, the corresponding values of the original variables are obtained by:

$$X = F_x^{-1}(U_x) \tag{13}$$

$$Y = F_y^{-1}(U_y) \tag{14}$$

A more detailed description on how to compute environmental contours with copulas can be found in Montes-Iturrizaga and Heredia-Zavoni (2015). Defined the environmental contours, the individuation of a specific pair of variables associated to each contour is related to the type of application for which the contours are computed. Different application of environmental contours have been done. Mikulić and Parunov (2023) applied environmental contours on extreme vertical wave bending moments on oil tankers on the Adriatic Sea, Clarindo and Guedes Soares (2024) analyzed the relation between wave height and wave period on the US East Coast by taking the maximum wave height and the associated wave period and vice versa, Ross et al. (2020) studied the response of fixed and floating structures using both results from a response simulator and from a deterministic approach.

In the present work, a deterministic approach was applied for the selection of a pair of values of storm surge and wave height associated to each environmental contour. Since this work focuses on extreme water levels that can cause coastal flooding, the response of the system (R) is expressed in terms of the overall increase of the water level at the shoreline and it is computed as the sum of two flooding contributions as:

$$R = \eta_{ss} + \eta_w = \eta_{ss} + 0.188H_b = \eta_{ss} + 0.188H_s \tag{15}$$

where the two components are, respectively, the increase of sea level due to storm surge η_{ss} and the wave set-up η_w at the shoreline. The term of the wave set-up is evaluated as in Marini et al. (2022) from the formulation given by Bowen et al. (1968), which is valid for all beach profiles. As reported in Section 2.1.3, the maximum setup value depends on the local beach profile; therefore, to generalize, it has been evaluated at the shoreline in still water condition. The computation of the wave set-up at the still-water shoreline leads to $\eta_w = 0.188H_b$, where H_b is the breaking wave height. The value of the wave height at breaking depth depends on the site-specific wave-transformation processes, expressed by the shoaling k_s and refraction k_r coefficients (see Section 2.1.3). Since such coefficients varies within the range 0.7–1.5, for simplicity it has been assumed that their product $k_s k_r$ is equal to 1, so that the breaking wave height H_b coincides with the offshore significant wave height H_s, as reported in Eq. (15). Along each contour, the value of R is computed and the design condition is given by its maximum value.

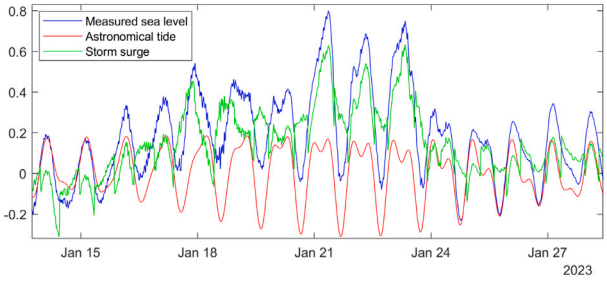

Fig. 4. Time series of measured sea level (blue) and computed astronomical tide (red) and storm surge during a high sea level event observed in Ancona in January 2023. (For interpretation of the references to color in this figure legend, the reader is referred to the web version of this article.)

3. Results and discussion

3.1. Results of bivariate statistical analysis

3.1.1. Application to Ancona site

In this section the application of the methodology is reported for the Ancona site. The same procedure is applied to all the other sites and the results are reported below. The sea level recordings of Ancona tide gauge were elaborated in order to extract the storm surge following the procedure of Section 2.3.1. The measured sea level in Ancona, with the reconstructed astronomical tidal and storm surge time series, are shown in Fig. 4. As reported in Fig. 3, the declustering procedure was applied to separate individual storm surge peaks.

As reported in Section 2.3.3 a site-specific choice of the best threshold for the main variable (storm surge) is made, while a representative threshold of the second variable (significant wave height) of 1 m was chosen for all the sites. Fig. 5 shows the plots for the choice of the threshold at Ancona site for the storm surge dataset. Panel a of Fig. 5 shows a linear trend for the MRL up to a threshold of 0.45 m. For larger values an almost horizontal slope is observed, together with a large increase of the confidence interval (CI) width. A similar increase in the CI width is observed for the GP parameters at $y_t = 0.45$ m (panels b and c). In panel d, a large spreading of NRMSE is observed at $y_t > 0.40$ m. This suggests that the threshold value must be set smaller than 0.4 m. In addition, the scale parameter has a slightly increasing trend from 0.20 m to 0.29 m, while it assumes almost constant values between 0.30 m and 0.40 m. In this range, minimum values of NRMSE are observed at $y_t = 0.30$ m and $y_t = 0.33$ m and the largest threshold of $y_t = 0.33$ m is chosen among the two values to exclude smaller storm surge events. In any case, due to the small differences between these statistical parameters, threshold values in the range between 0.30 m and 0.40 m are expected to give quite similar results.

Fig. 6 shows the results of the POT analysis in a probabilistic chart where the storm surge is plotted as a function of RP. The red circles of Fig. 6 represent the observed events, while the black line gives the storm surge values associated to different return periods for the Generalized Pareto distribution.

The final set of variable pairs for the Ancona site is represented by the red circles in Fig. 7a, where the less energetic wave conditions are drawn in gray (wave height smaller than 1 m).

The next step is to evaluate which extreme statistical distribution best fits the wave height data. Using RMSE as the criterion for the optimal fit, the Weibull distribution is found to be the best one for the wave height dataset of Ancona site. Fig. 7b shows the adaptation of the cumulative distribution function to the observed data. After determining the marginal distribution for the wave height (second variable), the joint distribution has been found by using a copula approach.

The copula-based analysis requires a tool to describe and graphically represent the joint behavior of the analyzed parameters. The environmental contours for the Ancona site are reported in Fig. 8. Each point along these contours has the same joint probability, meaning that they represent equally likely combinations of storm surge and wave height associated to different RPs from 1 to 200 years. The distribution of these points provides valuable information about the relationship between these two variables. Specifically, it is observed that larger wave heights are typically associated with higher storm surge values. This is crucial for understanding how storm surge and wave conditions interact during extreme weather events. For storm surge values just above the threshold level, the significant wave height exhibits considerable variability, ranging from 1.0 m to 4.5 m. This indicates that even small increases in storm surge can occur under a wide range of wave conditions, complicating predictions of extreme events. On the other hand, the data consistently show that higher storm surge values, particularly those exceeding 0.6 m, are associated with storms characterized by significant wave heights of at least 1.8 m.

The individuation of a specific pair of variables associated to each environmental contour is related to the type of application. In the present study the focus is the evaluation of extreme water levels that may cause coastal flooding. Therefore, the pairs of η_{ss} and H_s that maximizes the response of the system (R) for different return periods are computed by applying Eq. (15) and the relative line is traced over the graph (red line in Fig. 8).

3.1.2. Application to all sites

The analysis reported in Section 3.1.1 has been applied to the other sites in the Adriatic Sea (Fig. 2). Specific threshold values y_t of the storm surge data were found for the different sites; in particular, larger values of y_t were obtained by moving from South to North of the Adriatic Sea. As explained above, the same threshold value, equal to 1 m, was chosen as representative threshold of the significant wave height data for each site in the Adriatic Sea. A copula-based approach was followed for the identification of the joint relations between the two datasets (storm surge η_{ss} and significant wave height H_s) for each site and the relative environmental contours are computed. Therefore, the pairs of η_{ss} and H_s that maximizes the response of the system (R) are identified, as provided by Eq. (15) for different return periods RPs and for all 12 sites, as shown in Fig. 9. Different shape of environmental contours were found for the different sites, in particular Fig. 9 shows that very significant storm surge values, about 1.4 m for a 100-year return period, occur in the northern part of the Adriatic Sea (Venice and Trieste sites), significant values, about 1.0 m, in the north-central area (Ravenna, Ancona, Rovinj sites), quite significant values, about 0.8 m, in the central-eastern area (Zadar and Split), moderate values, about 0.6 m, in the central-southern area (Ortona, Vieste and Dubrovnik sites) while values smaller than 0.5 m are observed in the southern part (Bari and Otranto sites).

3.2. Maps of sea level contributions and joint significant wave height in the Adriatic Sea

The results of the bivariate statistical analysis applied to all the sites are summarized in Table 3, with the pairs of η_{ss} and H_s that maximize the response of the system (R) given by Eq. (15) for different return periods (red lines in Fig. 9). The other sea level contributions of Eq. (1) are computed at each site for different climate projections and reported in Table 3. Since one of the aims of the present study is to provide an estimate of both the sea level contributions and the extreme sea levels for the Adriatic Sea, different maps are computed for different climate projections and return periods. The graphical representation of sea level results for the whole Adriatic sea was achieved by applying the kriging interpolation (Matheron, 1963), that is a spatial interpolation method used to obtain predictions at unsampled locations based on observed geostatistical data.

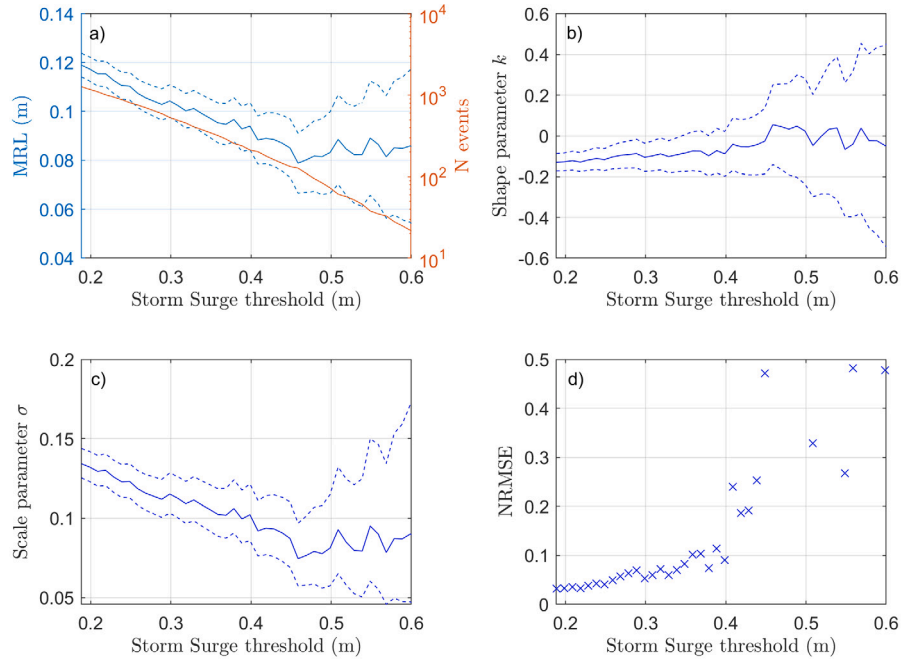

Fig. 5. Statistical parameters used to determine the storm surge threshold at the Ancona site. Panel (a): Mean Residual Life (MRL) plot with associated confidence intervals (blue) and the number of exceedances for each candidate threshold; panels (b) and (c): stability of the GP shape and scale parameters with their confidence intervals; panel (d): NRMSE values for the different thresholds. (For interpretation of the references to color in this figure legend, the reader is referred to the web version of this article.)

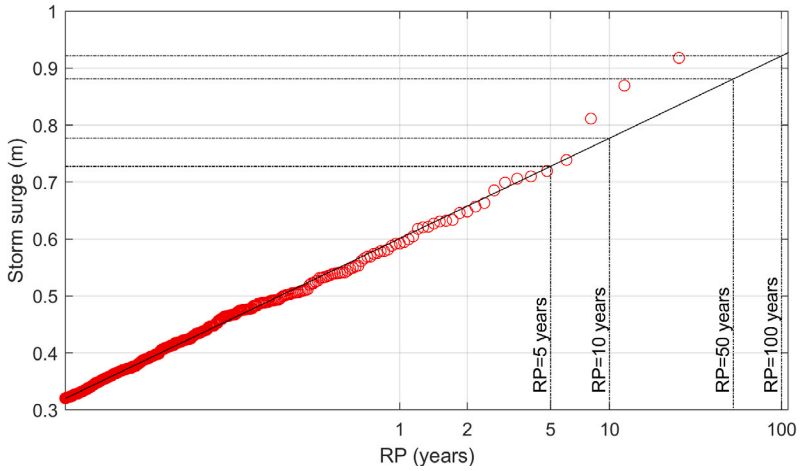

Fig. 6. Generalized Pareto distribution probabilistic chart. Red circles represent observed storm surge data while the black line represents the storm surge data from the probabilistic distribution. (For interpretation of the references to color in this figure legend, the reader is referred to the web version of this article.)

3.2.1. Sea level rise

Projections of sea level rise are taken from the NASA Sea Level Projection tool (https://sealevel.nasa.gov/ipcc-ar6-sea-level-projection-tool) of the IPCC 6th Assessment Report (Calvin et al., 2023). Two different climate scenarios are considered, namely SSP1-1.9 and SSP5-8.5. For these scenarios, the value of the sea level rise at each site is reported in Table 3, while Fig. 10 shows the maps of sea level rise for the whole Adriatic Sea. Under the more optimistic scenario SSP1-1.9 (panel a of Fig. 10), the projected sea level rise ranges from approximately 30 cm to 40 cm. The high-emission scenario SSP5-8.5 (panel b) suggests a nearly doubled rise, with values between 65 cm and 80 cm. Despite these differences in magnitude, the analysis reveals no clear spatial trend across various Adriatic sub-regions, especially for the SSP1-1.9 scenario, implying that the impact of climate change on sea level rise is uniformly distributed along the coastline rather than region-specific. The Venezia site is characterized by the larger values of sea level rise and it represents an hotspot in the Adriatic basin.

3.2.2. Astronomical tide

MHHW astronomical tide values are computed using the methodology of Section 2.3.1 for all the locations in Fig. 2. According to Vousdoukas et al. (2018), the results are independent of any return period or climate scenario (see Table 3 and Fig. 11). As expected from other studies (e.g.; Schwab and Rao, 1983; Medvedev et al., 2020), higher values of MHHW are obtained in the northern part of the Adriatic Sea (roughly between Trieste and Ravenna), ranging from 0.30 m to 0.40 m. The central part of the basin (from Zadar to Bari) settles on smaller but constant values of the maximum tidal levels (MHHW≈ 0.15 m). Smaller tidal levels are observed at the southern entrance of the basin, in Otranto, where the MHHW is equal to 0.10 m. These results

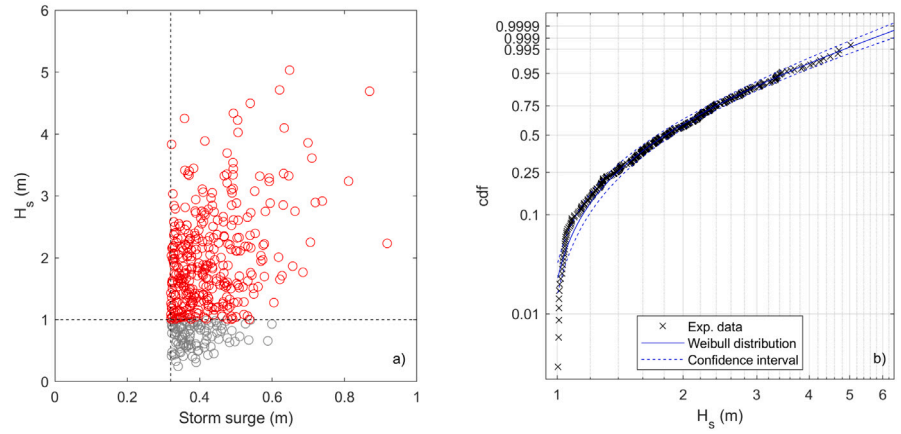

Fig. 7. Panel a: The red circles represent the pairs of associated storm surge and significant wave heights for the Ancona site, the gray circles are associated to less energetic conditions ($H_s < 1$ m); panel b: cumulative distribution function that best fits the experimental wave data. (For interpretation of the references to color in this figure legend, the reader is referred to the web version of this article.)

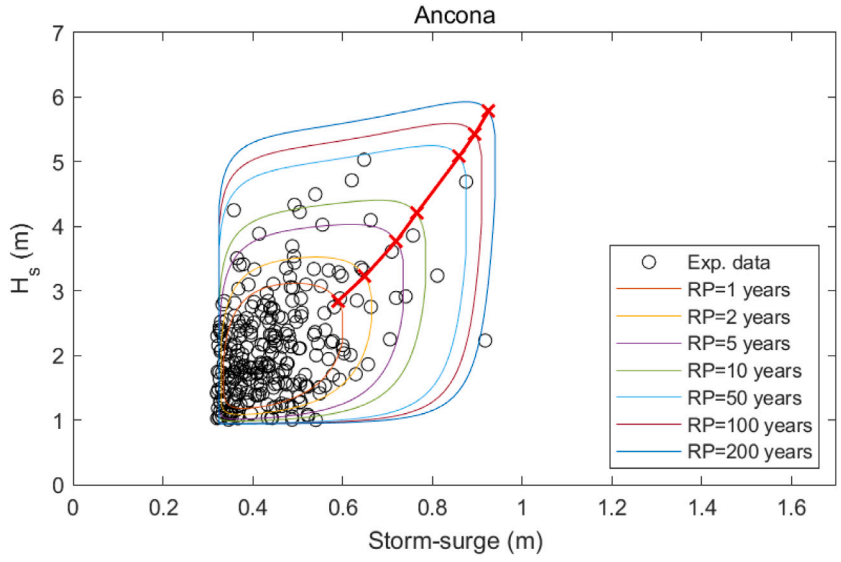

Fig. 8. Environmental contours between storm surge and significant wave height computed for different Return Periods in the Ancona site. (For interpretation of the references to color in this figure legend, the reader is referred to the web version of this article.)

Table 3
Main Sea Level components at the selected locations along the Adriatic coast: Sea Level Rise η_{slr} according to SSP1-1.9 and SSP5-8.5 scenarios; MHHW Astronomical tide η_t; Storm Surge η_{ss} and Wave Height H_s associated to the RPs of 10 and 100 years.

Location	η_{slr} SSP1-1.9 (m)	SSP5-8.5 (m)	η_t MHHW (m)	η_{ss} 10y (m)	100y (m)	H_s 10y (m)	100y (m)
Venezia	0.42	0.78	0.36	1.08	1.41	3.88	4.85
Trieste	0.31	0.67	0.39	1.02	1.19	3.19	4.00
Ravenna	0.32	0.69	0.28	0.82	0.90	3.45	4.19
Ancona	0.32	0.69	0.15	0.76	0.89	4.12	5.45
Ortona	0.34	0.70	0.15	0.53	0.60	3.42	4.61
Vieste	0.34	0.72	0.15	0.44	0.46	3.73	4.78
Bari	0.33	0.72	0.16	0.36	0.37	3.90	5.35
Otranto	0.35	0.74	0.10	0.40	0.45	4.24	5.66
Rovinj	0.28	0.64	0.29	0.78	0.93	2.89	3.93
Zadar	0.32	0.69	0.15	0.67	0.76	4.52	5.85
Split	0.29	0.66	0.14	0.61	0.73	2.77	3.60
Dubrovnik	0.33	0.71	0.16	0.47	0.50	3.74	4.82

confirm the overall micro-tidal nature of the basin, being its tidal range limited between 0 m and 2 m.

3.2.3. Storm surge

Extreme storm surge values are computed with the methodology of Section 2.3 for all the locations in Fig. 2. In order to evaluate the joint probability of storm surges and waves, the copula-based approach was used (Section 2.3.4) and the results are obtained in the form of environmental contours (Section 2.3.5). Similarly to the case of Ancona, the specific pairs of storm surge and wave height leading to the maximum values of R are computed with Eq. (15). The results are summarized in Table 3 and in Fig. 12. Maximum values of storm surge are expected to occur in the northern part of the Adriatic Sea, where values of $\eta_{ss} > 1m$ are also obtained for RP=10 years. The southern part of the basin is characterized by smaller values of storm surge, in the range of 35–50 cm for RP=10 years and 40–60 cm for RP=100 years. The extreme value analysis in the northern part of the basin leads to higher values, up to 1.40 m in Venice. These results are consistent with the findings of Vousdoukas et al. (2016) about the impacts of different climate scenarios on storm surge along the European coastline. Their study utilized a numerical model driven by wind and pressure

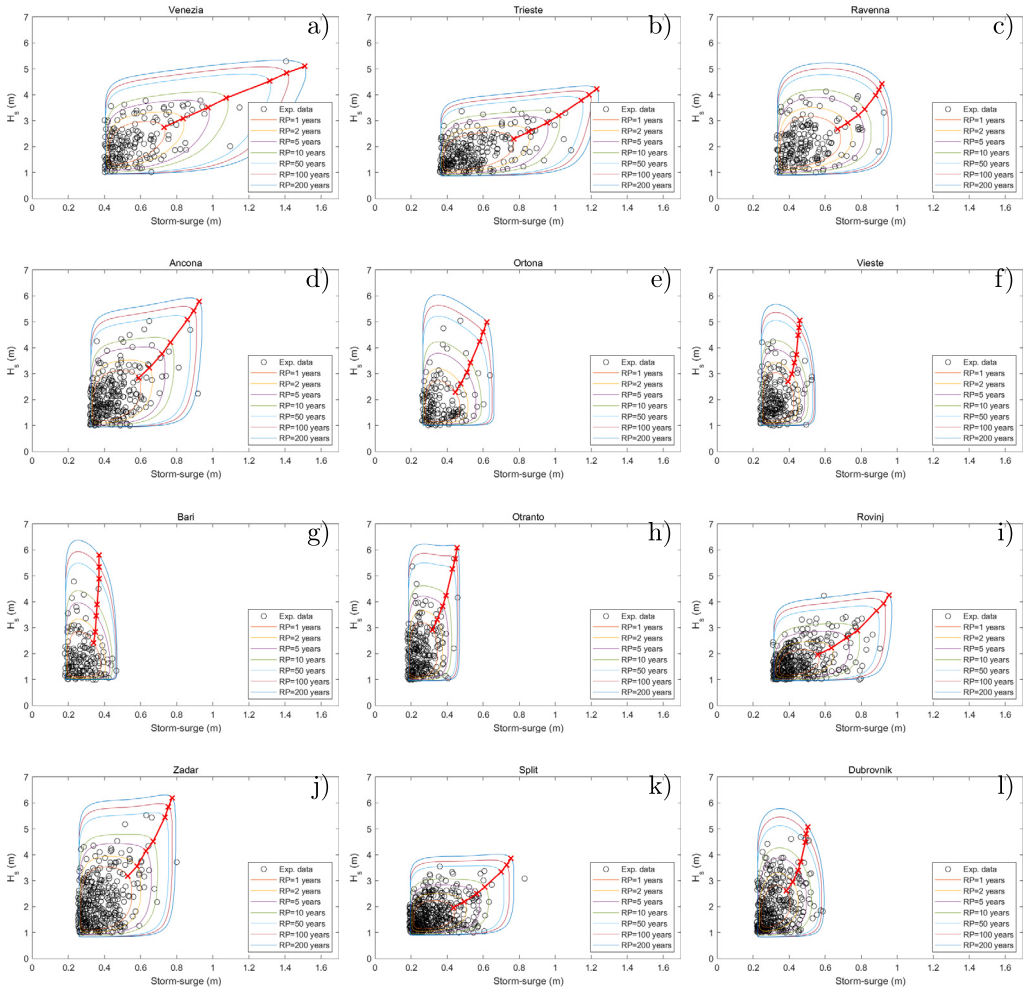

Fig. 9. Environmental contours obtained for the selected 12 sites: (a) Venezia, (b) Trieste, (c) Ravenna, (d) Ancona, (e) Ortona, (f) Vieste, (g) Bari, (h) Otranto, (i) Rovinj, (j) Zadar, (k) Split, (l) Dubrovnik. (For interpretation of the references to color in this figure legend, the reader is referred to the web version of this article.)

fields, incorporating a bias correction procedure. The site of Venice was selected as a representative location for the Central Mediterranean Sea. For this location, the extreme storm surge distribution appears largely independent of the considered climate scenario, with storm surge values of approximately 1.37 m for 10-years RP and 1.49 m for 100-year RP. These values align reasonably well with those obtained in this study (Table 3), which reports slightly lower values (1.08 m for RP10 and 1.41 m for RP100). The primary factor contributing to this discrepancy is likely the type of data used in the analysis for the storm surge dataset. In the present study, measured data were used for the extreme statistical analysis, while Vousdoukas et al. (2016) relied on a numerical model. Their work highlights the importance of accurately downscaling wind and pressure inputs to regional and local scales, as storm surge in shallow areas is predominantly driven by wind. Consequently, a detailed representation of the wind field is essential. Additionally, the use of a regular grid with a resolution of 0.2° (approximately 16 × 22 km in the Adriatic Sea region) in Vousdoukas et al. (2016) may not be sufficient for modeling the Adriatic Sea, a relatively small basin.

3.2.4. Wave height

The procedure to determine extreme wave heights that can occur during important storm surge events was already described in Sections 2.3 and 3.2.3. The results are reported in Table 3 and, in graphical form, in Fig. 13. As shown in Fig. 13, there is no a clear pattern of wave height distribution in the Adriatic Sea. Maximum values are observed to occur in the central part of the basin, between Ancona and Zadar, and in its southern entrance. This result can be explained by the fact that these sites have a double exposition to waves, both from north-west and from south-east. Indeed, the sites in the northern part of the domain are mainly influenced by waves propagating from south-east. When extreme storm surges are generated by storms directed southward, the associated wave height will be smaller, thus reducing the overall extreme value that characterize such sites. towards the southern part of the sea, a nearly uniform pattern emerges. In fact, the fetch for waves propagating from the north-west increases, while the fetch of waves from the south-east decreases. On the contrary areas characterized by a strong bidirectional wave climate, such as those in the middle Adriatic Sea (e.g. Ancona and Zadar) are subjected by a larger probability occurrence of joint events. An exception is the case of Split, where the point chosen for wave analysis is influenced by the significant presence of islands that strongly reduce wave activity from the south-east. However, the choice of an alternative point outside the influence of these islands would resulted in a location too far from the corresponding tide gauge, making the analysis less representative (as reported in Section 2.2.3 the wave stations are all located at a distance within the range 10 km–50 km from the relative tide-gauge). A similar

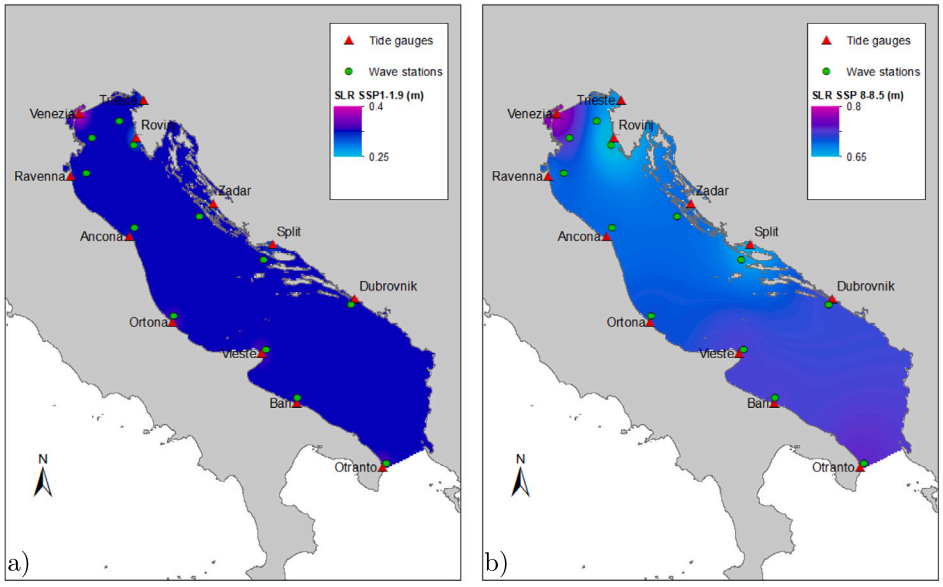

Fig. 10. Maps of sea level rise in the Adriatic basin for two different IPCC scenarios. Panel (a) SSP1-1.9, panel (b) SSP5-8.5. (For interpretation of the references to color in this figure legend, the reader is referred to the web version of this article.)

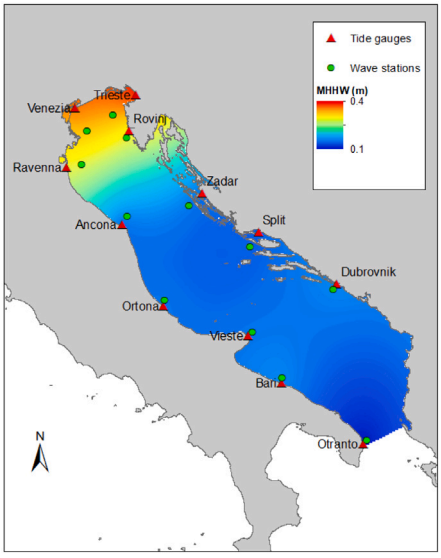

Fig. 11. Map of the Mean Higher High Water (MHHW) sea levels in the Adriatic basin. (For interpretation of the references to color in this figure legend, the reader is referred to the web version of this article.)

but less pronounced effect is observed in Ortona, where slightly lower values of wave height are observed due to the presence of the Gargano Promontory. In Otranto, the wave climate becomes bidirectional once again. The fetch for waves propagating from the north-west reaches its maximum length, while waves from the south are generated in the Ionian Sea, which extends beyond the Otranto Channel.

3.3. Maps of extreme sea levels in the Adriatic Sea

In this section maps of extreme sea levels evaluated for different return periods and climate change scenarios are provided. Eq. (1) summarizes the contributions to Extreme Sea Levels (ESLs) η, which include the mean sea level η_{msl}, the astronomical tide η_t, the sea level rise η_{slr}, the storm surge η_{ss} and wave effects η_w. When assessing coastal flooding, the impact of waves should be included by adding the wave setup η_w, as reported in Eq. (15) to consider the joint occurrence of different phenomena responsible of the extreme sea levels referred to different return periods..

To standardize the results across different sites in the Adriatic Sea, the mean sea level η_{msl} was removed from the analysis, because data from different tide gauge networks were used. For a local evaluation of sea levels, this value must be added to the ESLs computed in this section to correctly align with the local reference system.

Astronomical tide, in terms of MHHW, has been considered in all scenarios. Storm surge has also been evaluated in all scenarios, referred to two return periods (10 and 100 years). Wave contribution has been considered in some scenarios for two different return periods (10 and 100 years). Additionally, three climate change scenarios have been considered: no sea level rise ($\eta_{slr} = 0m$), sea level rise as predicted in SSP1-1.9 projections and sea level rise as predicted by SSP5-8.5 projections.

The ESL scenarios are summarized in Table 4. Specifically, *ESL1* includes only the contributions of astronomical tide and storm surge for a 10-year return period, while *ESL2* adds the effect of the corresponding wave conditions in terms of set-up. Similarly, *ESL3* and

Table 4
Extreme Sea Levels scenarios considering the contribution of sea level rise (SLR), astronomical tide (MHHW), storm surge and set-up induced by waves. The statistical values of the ESLs (minimum, maximum, mean and standard deviation) in the Adriatic Sea are also reported.

Name	SLR	MHHW	Surge	Wave	η_{min} (m)	η_{max} (m)	η_{mean} (m)	$\eta_{st\,dev}$ (m)
ESL1	0	✓	RP10	×	0.49	1.45	0.75	0.22
ESL2	0	✓	RP10	RP10	1.17	2.16	1.45	0.21
ESL3	0	✓	RP100	×	0.54	1.78	0.84	0.27
ESL4	0	✓	RP100	RP100	1.50	2.69	1.76	0.25
ESL1	SSP1-1.9	✓	RP10	×	0.84	1.87	1.08	0.22
ESL2	SSP1-1.9	✓	RP10	RP10	1.50	2.58	1.78	0.21
ESL3	SSP1-1.9	✓	RP100	×	0.87	2.20	1.16	0.27
ESL4	SSP1-1.9	✓	RP100	RP100	1.84	3.11	2.09	0.25
ESL1	SSP5-8.5	✓	RP10	×	1.23	2.23	1.45	0.21
ESL2	SSP5-8.5	✓	RP10	RP10	1.89	2.94	2.15	0.21
ESL3	SSP5-8.5	✓	RP100	×	1.26	2.56	1.54	0.26
ESL4	SSP5-8.5	✓	RP100	RP100	2.21	3.47	2.46	0.24

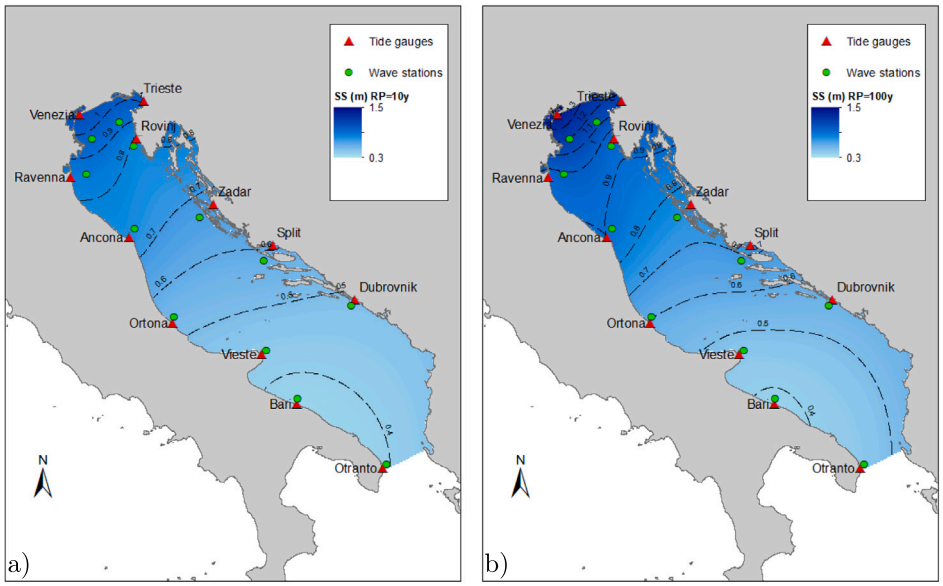

Fig. 12. Maps and contours of sea levels due to storm surge in the Adriatic basin for different Return Periods. Panel a: 10 years, panel b: 100 years. (For interpretation of the references to color in this figure legend, the reader is referred to the web version of this article.)

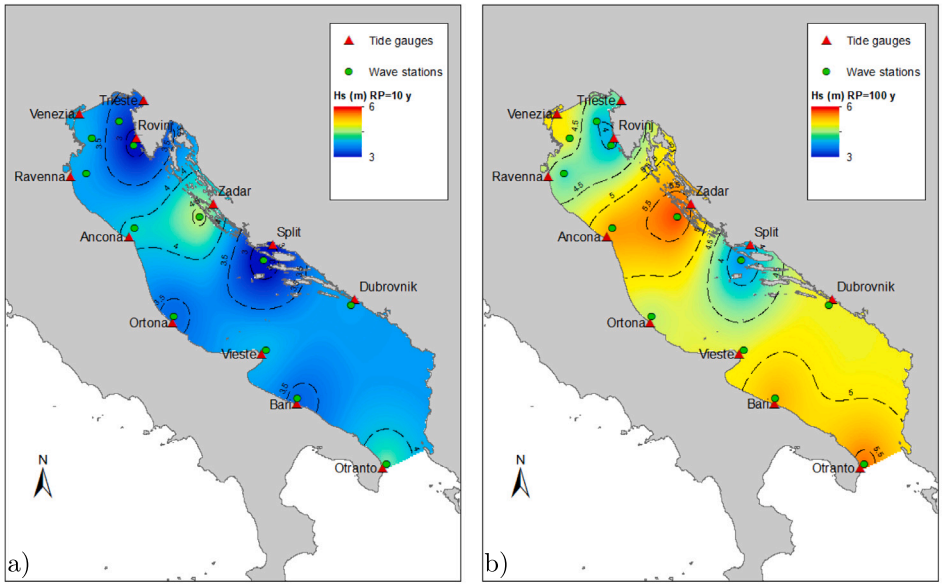

Fig. 13. Maps and contours of wave heights associated to extreme storm surge levels in the Adriatic basin for different Return Periods. Panel a: 10 years, panel b: 100 years. (For interpretation of the references to color in this figure legend, the reader is referred to the web version of this article.)

ESL4 correspond to the 100-year return period. These four scenarios do not account for sea level rise due to climate change. The same four scenarios are re-analyzed to incorporate the effects of climate trends, considering the SSP1-1.9 and SSP5-8.5 climate projections.

Fig. 14 presents the results for scenarios that do not account for the effects of climate change. These results confirm the vulnerability of the northern Adriatic Sea to storm surges and waves, as this region exhibits the highest extreme sea levels. As expected, *ESL3* and *ESL4* show higher levels compared to *ESL1* and *ESL2*, respectively, since they refer to larger RPs. On average, the extreme sea level with the 100-year return period is 10%–20% higher than the sea level relative to the 10-year return period.

For coastal flooding problems, the impact of waves on flooding levels is accounted for using Eq. (15). Waves significantly amplify water levels. In scenarios *ESL2* and *ESL4*, where wave effects are included, the sea levels are approximately double those corresponding to the same scenarios without waves (*ESL1* and *ESL3*). For a more detailed analysis of the water levels induced by these forcings across the entire Adriatic Sea, statistical parameters were calculated using all the points employed in the interpolation over the domain. Specifically, the minimum and maximum values (η_{min} and η_{max}, respectively), the mean (η_{mean}) and the standard deviation ($\eta_{st\ dev}$) were computed. The calculated indicators are summarized in Table 4. Independently of the considered return period, the lowest ESL values are observed near Otranto for the scenarios without waves, as both storm surge and tide contributions are minimal in this area. However, when waves are accounted for, the location of the minimum values shifts northward, as Otranto is more exposed to waves originating from the Ionian Sea. Maximum ESL values are consistently observed in the northern part of the basin, near Venice. However, as discussed in Section 3.2.4, the effect of waves is more pronounced in the central part of the basin. This results in a more uniform ESL field, as evidenced by lower standard deviation

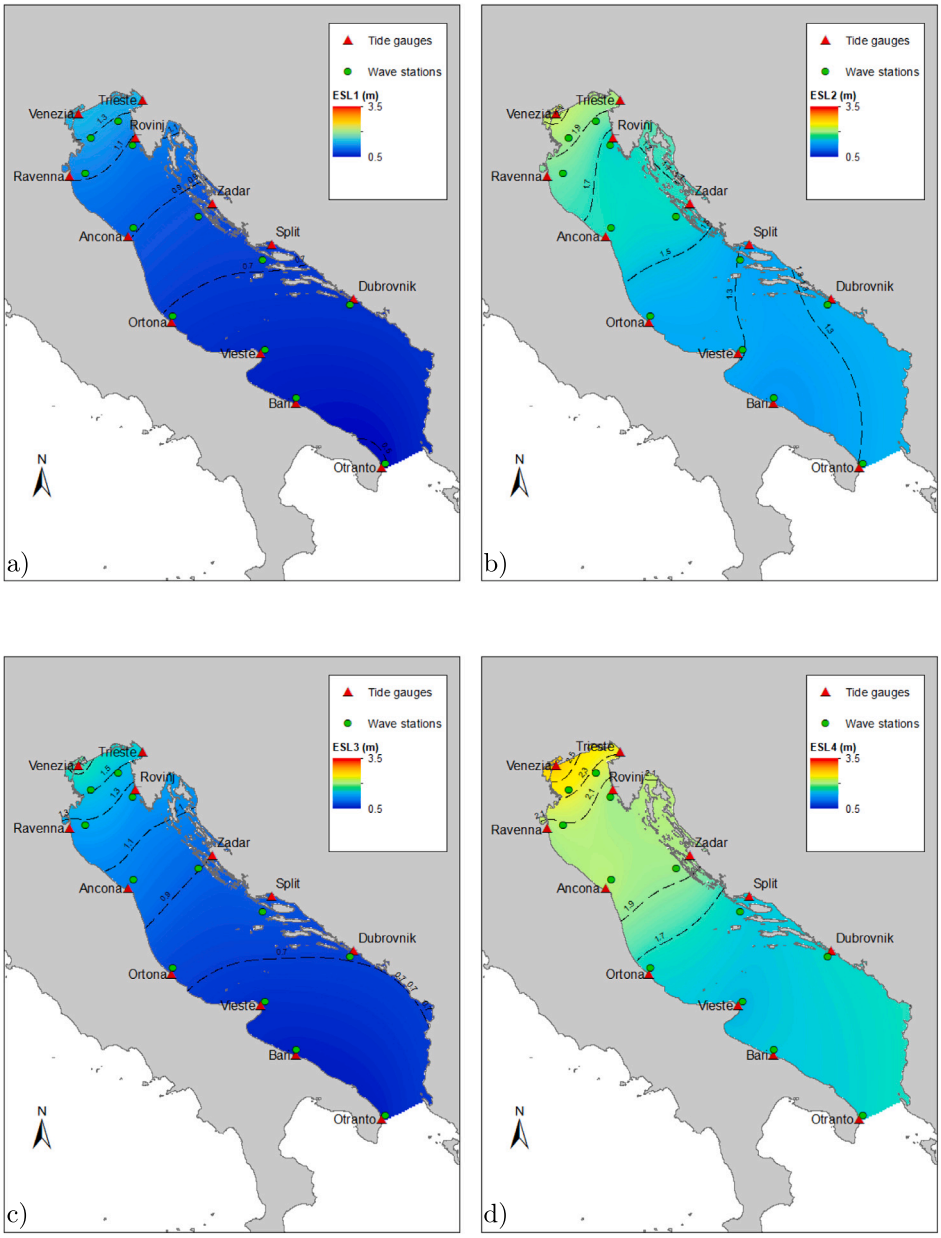

Fig. 14. Extreme Sea Level maps and contours in the Adriatic Sea for scenarios without the effect of climate change: *ESL1* (panel a), *ESL2* (panel b), *ESL3* (panel c) and *ESL4* (panel d). (For interpretation of the references to color in this figure legend, the reader is referred to the web version of this article.)

values obtained for scenarios *ESL2* and *ESL4* (with waves) compared to *ESL1* and *ESL3* (without waves), respectively. The ESLs maps with wave contribution (e.g. ESL2 and ESL4 scenarios) are obtained by assuming the product of shoaling k_s and refraction k_r coefficients equal to 1 (see Section 2.1.3). As a preliminary and general assessment of coastal flooding due to extreme sea levels, such assumption can be considered reasonable. However, for a more accurate assessment of ESLs, a local computation of the wave setup η_w, and thus of the breaking wave height H_b, would be beneficial, as wave-transformation processes from deep water to the breaking depth are strongly influenced by site-specific conditions (wave direction, wave period, breaking water depth, bathymetry and emerged beach profile). In these cases, the local wave-setup contribution can be assessed by using the offshore wave height reported in the H_s maps (Fig. 13) to derive the breaking wave height H_b at the specific site, and then adding such contribution η_w to the maps that do not include it (e.g. ESL1 and ESL3 scenarios, respectively reported in panels a and c of Fig. 14). The same considerations are also valid for those scenarios which include the sea level η_{slr} rise contribution. Indeed, to provide a comprehensive assessment, the effect of climate change has been also taken into account. Starting from the scenarios that include wave contributions (*ESL2* and *ESL4*), the impact of climate change is analyzed by considering the SSP1-1.9 and SSP5-8.5 projections of the IPCC. The results across the Adriatic basin is presented in Fig. 15, where panels (a) and (b) show the ESL for the 10-years return period while panels (c) and (d) refer to 100-years RP. Left panels refers to SSP1-1.9 and right panels to SSP5-8.5. The SSP1-1.9 scenarios exhibit a relatively homogeneous pattern across the Adriatic basin, with slightly higher values obtained in Venice (Fig. 15a). In contrast, the SSP5-8.5 scenarios show greater spatial variability, with the highest levels expected along the Italian coast and the lowest values obtained near Rovinj and Split (Fig. 10b). As a result, for the SSP1-1.9 scenarios, the sea levels ESL2 and ESL4 (panels a–c of Fig. 15) closely resemble the corresponding ones without the climate change effect (panels b–d of Fig. 14), but with values approximately 33 cm higher on

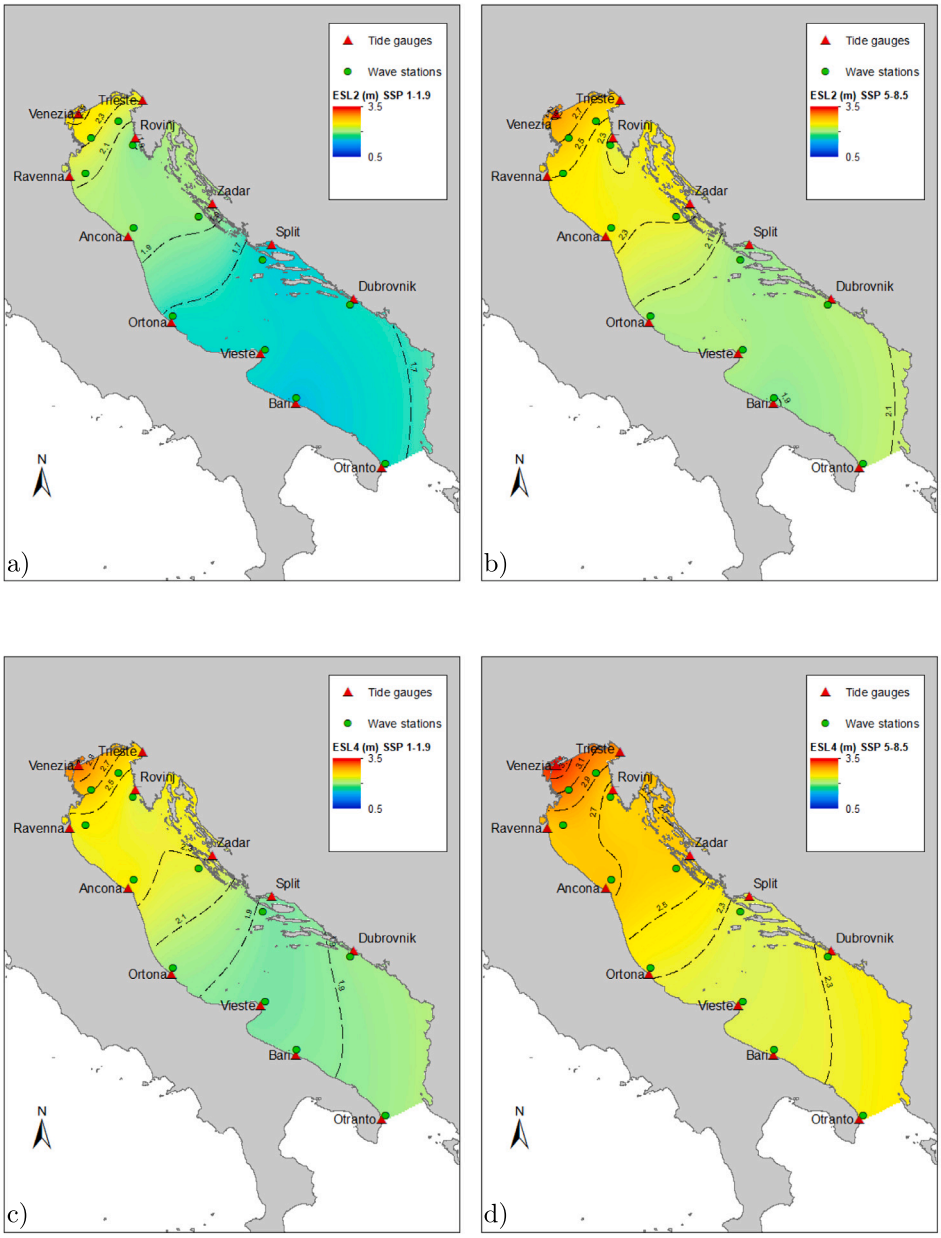

Fig. 15. Extreme Sea Level maps and contours in the Adriatic Sea for scenario *ESL2* with SSP1-1.9 (panel a) and SSP5-8.5 (panel b), and for scenario *ESL4* with SSP1-1.9 (panel c) and SSP5-8.5 (panel d). (For interpretation of the references to color in this figure legend, the reader is referred to the web version of this article.)

average. The difference in standard deviation between these two sets of scenarios is minimal, approximately 0.5–1 mm, which underscores the relatively uniform impact of the SSP1-1.9 scenario across the basin. For the SSP5-8.5 scenario, the standard deviation of the ESL varies by an average of 7–8mm compared to the baseline, reflecting the higher spatial variability of this scenario. This variability highlights the greater uncertainty and localized differences in sea level rise across the basin. As a result, the Adriatic Sea can be divided into three main regions based on the obtained sea level patterns. The northern part, extending slightly south of Ancona and Zadar, is characterized by the highest sea levels, where the Venice area stands out as a hotspot exhibiting the maximum values. Moving southward, the central part of the basin, extending roughly to Bari and Dubrovnik, shows lower ESL values on average. Finally, in the southern part of the Sea, towards Otranto, sea levels rise due to the influence of the Ionian Sea, which contributes to the local increase in water levels due to the incoming wave action.

4. Conclusions

The present study provides an effective coastal flooding risk assessment along the Adriatic coast, providing maps of both sea level contributions and of extreme sea level ESLs for different return periods and two IPPC climate change scenarios (SSP1-1.9 and SSP5-8.5). Moreover, the results enable valuable support for decision-makers and for the design of adaptation measures to address climate-driven extreme events.

The results of the bivariate statistical analyses applied to the 12 selected sites in the Adriatic Sea show that very high storm-surge values, about 1.4 m for a 100-years return period, occur in the northern part of the Adriatic Sea (Venice and Trieste). Significant values of about 1.0 m are found in the north-central area (Ravenna, Ancona, Rovinj), quite high values of about 0.8 m in the central-eastern area (Zadar and Split), and moderate values of about 0.6 m in the central-southern area

(Ortona, Vieste, Dubrovnik), while values below 0.5 m are observed in the southern part (Bari and Otranto). Incorporating wave contributions to the storm surge results significantly alters ESL distributions. Scenarios that include waves (*ESL2* and *ESL4*) — particularly relevant for coastal flooding evaluations — show levels significantly larger with respect to those without waves (*ESL1* and *ESL3*). Indeed, the findings of this study highlight the critical interplay between storm surge and wave height in determining extreme sea levels (ESLs) in the Adriatic Sea. Maximum ESLs are obtained in the northern Adriatic, with Venice identified as a hotspot due to the amplification effects of resonant mechanisms and local wind-driven processes. The results confirm that wave contributions can substantially double the extreme water levels. Significant increases in ESLs are observed between Ancona and Zadar, as well as near the southern Adriatic entrance at Otranto, where larger associated wave heights are found because these sites are characterized by a stronger bi-directional wave climate. This result highlights the need for a bivariate approach to fully capture the joint occurrence of storm events.

Statistical indicators calculated across the entire Adriatic domain confirm these patterns: the highest ESLs are observed in Venice, while the lowest values are found in Otranto, unless wave activity driven by the Ionian Sea is considered. For scenarios accounting for climate change, the SSP1-1.9 scenario increases ESLs by about 33 cm on average, with minimal changes in variability. Conversely, the SSP5-8.5 scenario amplifies both absolute levels and spatial variability, with a notable increase in standard deviation compared to baseline conditions. Projected sea level rise due to climate change is another key factor exacerbating coastal risks. Under the SSP1-1.9 scenario, sea levels are expected to rise by 30–40 cm, while the more pessimistic SSP5-8.5 scenario predicts increases of 65–80 cm. Notably, Venice consistently emerges as a focal point, exhibiting the highest sea level rise within the basin. Despite these increases, the SSP1-1.9 scenario shows no significant spatial trends, suggesting that the impact of sea level rise may be uniformly distributed across the basin. In contrast, the SSP5-8.5 scenario leads to greater spatial variability, with the highest levels along the northern coastline (mainly at the Italian side) and relatively lower values in the south-eastern area.

CRediT authorship contribution statement

Sara Corvaro: Writing – review & editing, Supervision, Methodology, Investigation, Conceptualization. **Francesco Marini:** Writing – review & editing, Writing – original draft, Methodology, Investigation, Formal analysis, Data curation, Conceptualization. **Stefania Rocchi:** Writing – review & editing, Methodology, Formal analysis. **Carlo Lorenzoni:** Writing – review & editing, Supervision, Conceptualization.

Declaration of competing interest

The authors declare that they have no known competing financial interests or personal relationships that could have appeared to influence the work reported in this paper.

Data availability

Data will be made available on request.

References

Aas, K., Czado, C., Frigessi, A., Bakken, H., 2009. Pair-copula constructions of multiple dependence. Insurance Math. Econom. 44 (2), 182–198. http://dx.doi.org/10.1016/j.insmatheco.2007.02.001.

Arns, A., Dangendorf, S., Jensen, J., Talke, S., Bender, J., Pattiaratchi, C., 2017. Sea-level rise induced amplification of coastal protection design heights. Sci. Rep. 7 (40171), http://dx.doi.org/10.1038/srep40171.

Bader, B., Yan, J., Zhang, X., 2017. Automated selection of r for the r largest order statistics approach with adjustment for sequential testing. Stat. Comput. 27, http://dx.doi.org/10.1007/s11222-016-9697-3.

Baldoni, A., Marini, F., Filomena, G., Parlani, S., Brocchini, M., 2025. Climate change-driven coastal flooding in the mid adriatic sea and adaptation of coastal defense structures. Estuar. Coast. Shelf Sci. 326, 109535. http://dx.doi.org/10.1016/j.ecss.2025.109535.

Bernardara, P., Andreewsky, M., Benoit, M., 2011. Application of regional frequency analysis to the estimation of extreme storm surges. J. Geophys. Res. 116, C02008.

Bernier, N.B., Thompson, K.R., 2007. Tide-surge interaction off the east coast of Canada and northeastern United States. J. Geophys. Res.: Ocean. 112 (C6), http://dx.doi.org/10.1029/2006JC003793.

Bowen, A.J., Inman, D.L., Simmons, V.P., 1968. Wave 'set-down' and set-up. J. Geophys. Res. 73, 2569–2577.

Burvingt, O., Masselink, G., Russell, P., Scott, T., 2017. Classification of beach response to extreme storms. Geomorphology 295, 722–737. http://dx.doi.org/10.1016/j.geomorph.2017.07.022.

Callahan, J.A., Leathers, D.J., 2021. Estimation of return levels for extreme skew Surge Coastal flooding events in the delaware and chesapeake bays for 1980–2019. Front. Clim. 3, http://dx.doi.org/10.3389/fclim.2021.684834.

Calvin, K., Dasgupta, D., Krinner, G., Mukherji, A., Thorne, P.W., Trisos, C., Romero, J., Aldunce, P., Barrett, K., Blanco, G., Cheung, W.W., Connors, S., Denton, F., Diongue-Niang, A., Dodman, D., Garschagen, M., Geden, O., Hayward, B., Jones, C., Jotzo, F., Krug, T., Lasco, R., Lee, Y.-Y., Masson-Delmotte, V., Meinshausen, M., Mintenbeck, K., Mokssit, A., Otto, F.E., Pathak, M., Pirani, A., Poloczanska, E., Pörtner, H.-O., Revi, A., Roberts, D.C., Roy, J., Ruane, A.C., Skea, J., Shukla, P.R., Slade, R., Slangen, A., Sokona, Y., Sörensson, A.A., Tignor, M., van Vuuren, D., Wei, Y.-M., Winkler, H., Zhai, P., Zommers, Z., Hourcade, J.-C., Johnson, F.X., Pachauri, S., Simpson, N.P., Singh, C., Thomas, A., Totin, E., Alegría, A., Armour, K., Bednar-Friedl, B., Blok, K., Cissé, G., Dentener, F., Eriksen, S., Fischer, E., Garner, G., Guivarch, C., Haasnoot, M., Hansen, G., Hauser, M., Hawkins, E., Hermans, T., Kopp, R., Leprince-Ringuet, N., Lewis, J., Ley, D., Ludden, C., Niamir, L., Nicholls, Z., Some, S., Szopa, S., Trewin, B., van der Wijst, K.-I., Winter, G., Witting, M., Birt, A., Ha, M., 2023. IPCC, 2023: Climate Change 2023: Synthesis Report. Contribution of Working Groups I, II and III to the Sixth Assessment Report of the Intergovernmental Panel on Climate Change [Core Writing Team, H. Lee and J. Romero (eds.)]. IPCC, Geneva, Switzerland. Intergovernmental Panel on Climate Change (IPCC), http://dx.doi.org/10.59327/ipcc/ar6-9789291691647.

Clarindo, G., Guedes Soares, C., 2024. Environmental contours of sea states by the I-FORM approach derived with the burr-lognormal statistical model. Ocean Eng. 291, 116315. http://dx.doi.org/10.1016/j.oceaneng.2023.116315.

Coblenz, M., 2021. MATVines: A vine copula package for MATLAB. Revstat Stat. J. 14, http://dx.doi.org/10.1016/j.softx.2021.100700.

Coco, G., Senechal, N., Rejas, A., Bryan, K., Capo, S., Parisot, J., Brown, J., MacMahan, J., 2014. Beach response to a sequence of extreme storms. Geomorphology 204, 493–501. http://dx.doi.org/10.1016/j.geomorph.2013.08.028.

Cushman-Roisin, B., Beckers, J.-M., 2011. Introduction to Geophysical Fluid Dynamics: Physical and Numerical Aspects. Academic Press.

Cushman-Roisin, B., Gacic, M., Poulain, P.-M., Artegiani, A., 2013. Physical Oceanography of the Adriatic Sea: Past, Present and Future. Springer Science & Business Media.

Davison, A.C., Smith, R.L., 2018. Models for exceedances over high thresholds. J. R. Stat. Soc. Ser. B Stat. Methodol. 52 (3), 393–425. http://dx.doi.org/10.1111/j.2517-6161.1990.tb01796.x.

de Vries, H., Breton, M., de Mulder, T., Krestenitis, Y., Ozer, J., Proctor, R., Ruddick, K., Salomon, J.C., Voorrips, A., 1995. A comparison of 2D storm surge models applied to three shallow European seas. Environ. Softw. 10 (1), 23–42. http://dx.doi.org/10.1016/0266-9838(95)00003-4.

Dean, R.G., 1991. Equilibrium beach profiles: Characteristics and applications. J. Coast. Res. 7 (1), 53–84.

Dean, R.G., Dalrymple, R.A., 1991. Water wave mechanics for engineers and scientists. 105.

Det Norske Veritas, 2021. DNV-RP-c205. Environmental conditions and environmental loads. In: DNV AS.

Eckert-Gallup, A.C., Sallaberry, C.J., Dallman, A.R., Neary, V.S., 2016. Application of principal component analysis (PCA) and improved joint probability distributions to the inverse first-order reliability method (I-FORM) for predicting extreme sea states. Ocean Eng. 112, 307–319. http://dx.doi.org/10.1016/j.oceaneng.2015.12.018.

Furlan, E., Pozza, P.D., Michetti, M., Torresan, S., Critto, A., Marcomini, A., 2021. Development of a multi-Dimensional Coastal vulnerability index: Assessing vulnerability to inundation scenarios in the Italian coast. Sci. Total Environ. 772, 144650. http://dx.doi.org/10.1016/j.scitotenv.2020.144650.

Galiatsatou, P., Prinos, P., 2016. Joint probability analysis of extreme wave heights and storm surges in the aegean sea in a changing climate. E3S Web Conf. 7, 02002. http://dx.doi.org/10.1051/e3sconf/20160702002.

van Gent, M.R., 2019. Climate adaptation of coastal structures. Proc. the SCACR19—9th Short Course/Conference Appl. Coast. Res. Bari, Italy 9–11.

Goda, Y., 2010. Random seas and design of maritime structures. In: Advanced Series on Ocean Engineering. vol. 33, World Scientific, http://dx.doi.org/10.1142/7425.

Grinsted, A., 2014. Tidal fitting toolbox. https://www.mathworks.com/matlabcentral/fileexchange/19099-tidal-fitting-toolbox,

Guess, F., Proschan, F., 1988. 12 mean residual life: Theory and applications. In: Quality Control and Reliability. In: Handbook of Statistics, vol. 7, Elsevier, pp. 215–224. http://dx.doi.org/10.1016/S0169-7161(88)07014-2.

Haixia, Z., Meng, C., Weihua, F., 2023. Joint probability analysis of storm surges and waves caused by tropical cyclones for the estimation of protection standard: a case study on the eastern coast of the leizhou peninsula and the island of Hainan in China. Nat. Hazards Earth Syst. Sci. 23 (8), 2697–2717. http://dx.doi.org/10.5194/nhess-23-2697-2023.

Huang, W., Dong, S., 2021. Joint distribution of significant wave height and zero-up-crossing wave period using mixture copula method. Ocean Eng. 219, 108305. http://dx.doi.org/10.1016/j.oceaneng.2020.108305, URL https://www.sciencedirect.com/science/article/pii/S0029801820312208.

Idier, D., Bertin, X., Thompson, P., Pickering, M.D., 2019. Interactions between mean sea level, tide, surge, waves and flooding: Mechanisms and contributions to sea level variations at the coast. Surv. Geophys. 40, 1603—-1630. http://dx.doi.org/10.1007/s10712-019-09549-5.

Jenkins, L.J., Haigh, I.D., Sifnioti, D.E., Pinto Rascon, J.A., Inayatillah, A., Kassem, H., 2025. Non-linear tide-surge interactions around the coast of the UK through the lens of tidal level, phase, and skew surge. Estuar. Coast. Shelf Sci. 321, 109323. http://dx.doi.org/10.1016/j.ecss.2025.109323.

Krvavica, N., Gržić, M.M., Innocenti, S., Matte, P., 2025. Impact of storm surge and power peaking on tidal-fluvial processes in microtidal neretva river estuary. Estuar. Coast. Shelf Sci. 318, 109227. http://dx.doi.org/10.1016/j.ecss.2025.109227.

Li, F., van Gelder, P., Ranasinghe, R., Callaghan, D., Jongejan, R., 2014. Probabilistic modelling of extreme storms along the dutch coast. Coast. Eng. 86, 1–13. http://dx.doi.org/10.1016/j.coastaleng.2013.12.009.

Lionello, P., Malanotte-Rizzoli, P., Boscolo, R., Alpert, P., Artale, V., Li, L., Luterbacher, J., May, W., Trigo, R., Tsimplis, M., Ulbrich, U., Xoplaki, E., 2006. The mediterranean climate: An overview of the main characteristics and issues. In: Lionello, P., Malanotte-Rizzoli, P., Boscolo, R. (Eds.), Mediterranean. In: Developments in Earth and Environmental Sciences, vol. 4, Elsevier, pp. 1–26. http://dx.doi.org/10.1016/S1571-9197(06)80003-0.

Makris, C.V., Tolika, K., Baltikas, V.N., Velikou, K., Krestenitis, Y.N., 2023. The impact of climate change on the storm surges of the mediterranean sea: Coastal sea level responses to deep depression atmospheric systems. Ocean. Model. 181, 102149. http://dx.doi.org/10.1016/j.ocemod.2022.102149.

Malačič, V., Viezzoli, D., Cushman-Roisin, B., 2000. Tidal dynamics in the northern adriatic sea. J. Geophys. Res.: Ocean. 105 (C11), 26265–26280. http://dx.doi.org/10.1029/2000JC900123.

Marini, F., Corvaro, S., Rocchi, S., Lorenzoni, C., Mancinelli, A., 2022. Semi-analytical model for the evaluation of shoreline recession due to waves and sea level rise. Water 14 (8), http://dx.doi.org/10.3390/w14081305, URL https://www.mdpi.com/2073-4441/14/8/1305.

Marini, F., Mancinelli, A., Corvaro, S., Rocchi, S., Lorenzoni, C., 2020. Coastal submerged structures adaptation to sea level rise over different beach profiles. Ital. J. Eng. Geol. Environ. SI, 87–98. http://dx.doi.org/10.4408/IJEGE.2020-01.S-10.

Martín, A., Wahl, T., Enriquez, A.R., Jane, R., 2024. Storm surge time series declustering using correlation analysis. Weather. Clim. Extrem. 45, 100701. http://dx.doi.org/10.1016/j.wace.2024.100701.

Matheron, G., 1963. Principles of geostatistics. Econ. Geol. 58 (8), 1246–1266. http://dx.doi.org/10.2113/gsecongeo.58.8.1246.

Matte, P., Jay, D.A., Zaron, E.D., 2013. Adaptation of classical tidal harmonic analysis to nonstationary tides, with application to river tides. J. Atmos. Ocean. Technol. 30 (3), 569–589. http://dx.doi.org/10.1175/JTECH-D-12-00016.1.

Mazas, F., Hamm, L., 2011. A multi-distribution approach to POT methods for determining extreme wave heights. Coast. Eng. 58 (5), 385–394. http://dx.doi.org/10.1016/j.coastaleng.2010.12.003.

Mazas, F., Hamm, L., 2017. An event-based approach for extreme joint probabilities of waves and sea levels. Coast. Eng. 122, 44–59. http://dx.doi.org/10.1016/j.coastaleng.2017.02.003, URL https://www.sciencedirect.com/science/article/pii/S0378383917300947.

Medvedev, I.P., Vilibić, I., Rabinovich, A.B., 2020. Tidal resonance in the adriatic sea: Observational evidence. J. Geophys. Res.: Ocean. 125 (8), http://dx.doi.org/10.1029/2020JC016168, e2020JC016168 2020JC016168.

Međugorac, I., Orlić, M., Janeković, I., Pasarić, Z., Pasarić, M., 2018. Adriatic storm surges and related cross-basin sea-level slope. J. Mar. Syst. 181, 79–90. http://dx.doi.org/10.1016/j.jmarsys.2018.02.005.

Međugorac, I., Pasarić, M., Güttler, I., 2020. Will the wind associated with the adriatic storm surges change in future climate? Theor. Appl. Climatol. 143 (1–2), 1–18. http://dx.doi.org/10.1007/s00704-020-03379-x.

Mikulić, A., Parunov, J., 2023. Environmental contours in the adriatic sea for design and analysis of marine structures. J. Mar. Sci. Eng. 11 (5), http://dx.doi.org/10.3390/jmse11050899.

Montes-Iturrizaga, R., Heredia-Zavoni, E., 2015. Environmental contours using copulas. Appl. Ocean Res. 52, 125–139. http://dx.doi.org/10.1016/j.apor.2015.05.007.

Nelsen, R.B., 2006. An Introduction to Copulas, second ed. Springer, New York, NY, USA.

Orlić, M., Pasarić, M., 2024. How to disentangle sea-level rise and a number of other processes influencing coastal floods? Rend. Lincei. Sci. Fis. E Nat. 35, 371–380. http://dx.doi.org/10.1007/s12210-024-01242-z.

Paprotny, D., Morales-Nápoles, O., Nikulin, G., 2016. Extreme sea levels under present and future climate: a pan-European database. E3S Web Conf. 7, 02001. http://dx.doi.org/10.1051/e3sconf/20160702001.

Paprotny, D., Vousdoukas, M., Morales-Nápoles, O., Jonkman, S.N., Feyen, L., 2020. Pan-European hydrodynamic models and their ability to identify compound floods. Nat. Hazards 101, 933–957. http://dx.doi.org/10.1007/s11069-020-03902-3.

Pasarić, M., Pasarić, Z., Orlić, M., 2000. Response of the adriatic sea level to the air pressure and wind forcing at low frequencies (0.01–0.1 cpd). J. Geophys. Res.: Ocean. 105, 11223–11523.

Pasquali, D., Di Risio, M., De Girolamo, P., 2015. A simplified real time method to forecast semi-enclosed basins storm surge. Estuar. Coast. Shelf Sci. 165, 61–69. http://dx.doi.org/10.1016/j.ecss.2015.09.002.

Pervan, M., Sepić, J., 2023. Analysis of the eastern adriatic sea level extremes. St-Open 4, 1–19. http://dx.doi.org/10.48188/so.4.10.

Petroliagkis, T.I., 2018. Estimations of statistical dependence as joint return period modulator of compound events – Part 1: Storm surge and wave height. Nat. Hazards Earth Syst. Sci. 18 (7), 1937–1955. http://dx.doi.org/10.5194/nhess-18-1937-2018, URL https://nhess.copernicus.org/articles/18/1937/2018/.

Phillips, J.D., 2024. Sequential changes in coastal plain rivers influenced by rising sea-level. Hydrology 11 (8), http://dx.doi.org/10.3390/hydrology11080124.

Ragno, E., Antonini, A., Pasquali, D., 2023. Investigating extreme sea level components and their interactions in the adriatic and tyrrhenian seas. Weather. Clim. Extrem. 41, 100590. http://dx.doi.org/10.1016/j.wace.2023.100590.

Rosenblatt, M., 1952. Remarks on a multivariate transformation. Ann. Math. Stat. 23 (3), 470–472. http://dx.doi.org/10.1214/aoms/1177729394.

Ross, E., Astrup, O.C., Bitner-Gregersen, E., Bunn, N., Feld, G., Gouldby, B., Huseby, A., Liu, Y., Randell, D., Vanem, E., Jonathan, P., 2020. On environmental contours for marine and coastal design. Ocean Eng. 195, 106194. http://dx.doi.org/10.1016/j.oceaneng.2019.106194.

Rueda, A., Camus, P., Tomás, A., Vitousek, S., Méndez, F., 2016. A multivariate extreme wave and storm surge climate emulator based on weather patterns. Ocean. Model. 104, 242–251. http://dx.doi.org/10.1016/j.ocemod.2016.06.008.

Ruić, K., Šepić, J., Mlinar, M., Međugorac, I., 2023. Contribution of high-frequency sea level oscillations to the adriatic sea level maxima. Nat. Hazards 116 (3), 3747–3777. http://dx.doi.org/10.1007/s11069-023-05834-0.

Saranyasoontorn, K., Manuel, L., 2004. Efficient models for wind turbine extreme loads using inverse reliability. J. Wind Eng. Ind. Aerodyn. 92 (10), 789–804. http://dx.doi.org/10.1016/j.jweia.2004.04.002.

Scarrott, C., MacDonald, A., 2012. A review of extreme value threshold estimation and uncertainty quantification. Revstat Stat. J. 10, 33–60. http://dx.doi.org/10.57805/revstat.v10i1.110.

Schmid, K., Hadley, B., Waters, K., 2014. Mapping and portraying inundation uncertainty of bathtub-type models. J. Coast. Res. 30 (3), 548–561. http://dx.doi.org/10.2112/JCOASTRES-D-13-00118.1.

Schwab, D.J., Rao, D.B., 1983. Barotropic oscillations of the mediterranean and adriatic seas. Tellus A: Dyn. Meteorol. Ocean. http://dx.doi.org/10.3402/tellusa.v35i5.11452.

Šepić, J., Pasarić, M., Međugorac, I., Vilibić, I., Karlović, M., Mlinar, M., 2022. Climatology and process-oriented analysis of the adriatic sea level extremes. Prog. Oceanogr. 209, 102908. http://dx.doi.org/10.1016/j.pocean.2022.102908.

Sklar, M., 1959. Fonctions de repartition an dimensions et leurs marges. Publ. Inst. Stat. Univ. Paris 8, 229–231.

Stephens, S.A., Bell, R.G., Haigh, I.D., 2020. Spatial and temporal analysis of extreme storm-tide and skew-surge events around the coastline of New Zealand. Nat. Hazards Earth Syst. Sci. 20 (3), 783–796. http://dx.doi.org/10.5194/nhess-20-783-2020.

Sweet, W., Dusek, G., Obeysekera, J., Marra, J., 2018. Patterns and Projections of High Tide Flooding along the U.S. Coastline Using a Common Impact Threshold. Technical Report, NOAA Technical Report NOS CO-OPS 86, http://dx.doi.org/10.7289/V5/TR-NOS-COOPS-086.

The MathWorks Inc., 2024. MATLAB version: 24.2.0 (r2024a). URL https://www.mathworks.com.

Vilibić, I., Orlić, M., Cupić, S., Domijan, N., Mihanović, H., Pasarić, M., Pasarić, Z., Srdelić, M., Strinić, G., 2005. A new approach to sea level observations in Croatia. Geofizika 22, 21–57.

Vousdoukas, M.I., Mentaschi, L., Voukouvalas, E., Verlaan, M., Feyen, L., 2017. Extreme sea levels on the rise along europe's coasts. Earth's Futur. 5 (3), 304–323. http://dx.doi.org/10.1002/2016ef000505.

Vousdoukas, M., Mentaschi, L., Voukouvalas, E., Verlaan, M., Jevrejeva, S., Jackson, L., Feyen, L., 2018. Global probabilistic projections of extreme sea levels show intensification of coastal flood hazard. Nat. Commun. 9, http://dx.doi.org/10.1038/s41467-018-04692-w.

Vousdoukas, M.I., Voukouvalas, E., Annunziato, A., Giardino, A., Feyen, L., 2016. Projections of extreme storm surge levels along Europe. Clim. Dyn. 47 (9), 3171–3190. http://dx.doi.org/10.1007/s00382-016-3019-5.

Wahl, T., Chambers, D.P., 2015. Evidence for multidecadal variability in US extreme sea level records. J. Geophys. Res.: Ocean. 120 (3), 1527–1544. http://dx.doi.org/10.1002/2014JC010443.

Williams, J., Horsburgh, K.J., Williams, J.A., Proctor, R.N.F., 2016. Tide and skew surge independence: New insights for flood risk. Geophys. Res. Lett. 43 (12), 6410–6417. http://dx.doi.org/10.1002/2016GL069522.

Winterstein, S., Ude, T., Cornell, C., Bjerager, P., Haver, S., 1993. Environmental parameters for extreme response: inverse FORM with omission factors. Proc. Intl. Conf. Struct. Saf. Reliab. (ICOSSAR93).

Zachary, S., Feld, G., Ward, G., Wolfram, J., 1998. Multivariate extrapolation in the offshore environment. Appl. Ocean Res. 20 (5), 273–295. http://dx.doi.org/10.1016/S0141-1187(98)00027-3.

Zheng, F., Westra, S., Sisson, S.A., 2013. Quantifying the dependence between extreme rainfall and storm surge in the coastal zone. J. Hydrol. 505, 172–187. http://dx.doi.org/10.1016/j.jhydrol.2013.09.054, URL https://www.sciencedirect.com/science/article/pii/S0022169413007075.